Title page

Maturation of telomere 3'-overhangs is linked to the replication stress response

Running title: Rad5 function in telomere replication

Erin E. Henninger[1], Pascale Jolivet[1], Emilie Fallet[1], Mohcen Benmounah[1], Zhou Xu[1,#], Stefano Mattarocci[1,°,*] and Maria Teresa Teixeira[1,*]

[1] Sorbonne Université, PSL, CNRS, UMR8226, Institut de Biologie Physico-Chimique, Laboratoire de Biologie Moléculaire et Cellulaire des Eucaryotes, F-75005 Paris, France

[#] Present address : Sorbonne Université, CNRS, UMR7238, Institut de Biologie Paris-Seine, Laboratory of Computational and Quantitative Biology, 75005 Paris, France

[°] Present address : DNA Repair and Chromosome Stability Team, Inserm U1274, Institut de Biologie François Jacob du Commissariat à l'Énergie Atomique et aux Énergies Alternatives, UMR E008 Université Paris-Saclay, Université de Paris, France

* correspondence to Stefano.mattarocci@inserm.fr; Teresa.teixeira@ibpc.fr

Abstract

Passage of the replication fork through telomeric repeats necessitates additional DNA processing by DNA repair factors, to regenerate the terminal 3'-overhang structure at leading telomeres. These factors are prevented from promoting telomeric recombination or fusion by an uncharacterized mechanism. Here we show that Rad5, a DNA helicase and ubiquitin ligase involved in the DNA damage tolerance pathway, participates in this mechanism. Rad5 is enriched at telomeres during telomere replication. Accelerated senescence seen in the absence of telomerase and Rad5, can be compensated for by a pathway involving the Rad51 recombinase and counteracted by the helicase Srs2. However, this pathway is only active at short telomeres. Instead, the ubiquitous activity of Rad5 during telomere replication is necessary for the proper reconstitution of the telomeric 3'-overhang, indicating that Rad5 is required to coordinate telomere maturation during telomere replication.

Key words

DNA processing/DNA replication/Helicases/Telomerase/Telomeres

Main Text

Introduction

Telomeres cap the ends of eukaryotic chromosomes (Jain & Cooper, 2010) and are composed of TG-rich repeat motifs of variable length. In budding yeast, telomeres have the degenerate sequence 5'-TG_{1-3}-3' and range from 200 to 400 bp in length, terminating in a 5-10 nt 3'-overhang on the strand running from the centromere to the telomere (Soudet *et al*, 2014; Wellinger & Zakian, 2012; Xu *et al*, 2013). The telomeric repeats recruit specific proteins to protect DNA ends from chromosome fusion and end degradation, by preventing the DNA damage response (DDR) at telomere ends. Telomeric proteins also control telomerase recruitment to chromosome ends. Without telomerase, telomeric DNA is lost at each passage of the replication fork, as the semiconservative replication machinery is unable to fully replicate the DNA ends.

In most human somatic tissues, which do not express telomerase, progressive telomere shortening is a major cause of senescence. Critically short telomeres activate a persistent DNA damage checkpoint; at the same time they prevent effective re-elongation by DNA repair activities (Campisi & d'Adda, 2007; Teixeira, 2013). Telomere-initiated senescence is bypassed in cancer cells by both suppressing the DNA damage checkpoint controlling replicative senescence and pathologically lengthening the telomeres (Artandi & DePinho, 2000). Conversely, abnormally short telomeres cause a spectrum of early and fatal degenerative syndromes, such as dyskeratosis congenita, pulmonary fibrosis, and bone marrow failure (Stanley & Armanios, 2015). Thus, homeostasis in many human organs depends on proper telomere function and shortening rate (Campisi & d'Adda, 2007; Hayflick, 1965). However, the mechanisms controlling telomere maintenance and shortening remain to be fully elucidated.

In many species the DNA-end replication problem arises when the replisome reaches the chromosome end and leading strand synthesis stops prematurely because there is no template at the 3'-overhang end structure (Lingner *et al*, 1995; Soudet *et al*., 2014). While

the RNA removal of the last Okazaki fragment in lagging strand synthesis is believed to be sufficient to reconstitute the 3'-overhang at lagging telomeres (Soudet *et al.*, 2014), additional DNA processing involving 5'-to-3' resection and CA-rich strand fill-in is required to regenerate the terminal 3'-overhang structure at leading telomeres (Diede & Gottschling, 1999, 2001; Giraud-Panis *et al*, 2010; Mirman *et al*, 2018; Wellinger *et al*, 1996; Wellinger *et al*, 1993; Wu *et al*, 2012; Zhao *et al*, 2009). The 5'-to-3' resection requires limited activation of the DNA damage checkpoint and the controlled activity of nucleases that act in double-strand break (DSB) processing to generate single stranded (ss)DNA (Lee *et al*, 2015; Sabourin & Zakian, 2008; Soudet *et al.*, 2014; Tong *et al*, 2015; Wellinger, 2014; Wu *et al.*, 2012). Current models for fill-in involve the loading of the $Cdc13^{CTC1}$-Stn1-Ten1 (CST) complex on the resulting telomeric ssDNA and stimulation of DNA alpha-primase polymerase activity to initiate DNA synthesis and define the 3'-overhang length (Giraud-Panis *et al.*, 2010; Lue *et al*, 2014; Mirman *et al.*, 2018). Therefore, the ends of chromosomes both trigger and limit DNA repair activities by an unclear coordination mechanism. Thus, despite its contribution to telomere length homeostasis, the control of 3'-overhang length and subsequent shortening rate thus remain to be understood.

Telomeric sequences share the characteristics of common fragile sites and pose similar problems for replication machinery, even in the absence of exogenous replication stress (Ivessa *et al*, 2002; Makovets *et al*, 2004; Miller *et al*, 2006; Moore *et al*, 2018; Sfeir *et al*, 2009). Telomeres are difficult to replicate, likely because of secondary structures at telomeric repeats or interactions with telomeric components, such as TERRA or telomeric proteins (Goto *et al*, 2015; Pfeiffer *et al*, 2013; Voineagu *et al*, 2009). Telomeres thus accumulate replication intermediates, which also recruit DNA repair factors. In yeasts, telomerase can efficiently re-extend short or dysfunctional telomeric sequences, provided a sufficient length of repeats is present (Matmati *et al*, 2020; Miller *et al.*, 2006; Negrini *et al*, 2007; Strecker *et al*, 2017). Consequently, telomerase-negative cells become dependent on pathways responding to replication stress to maintain cell viability, probably by preventing abrupt telomere shortening events (Abdallah *et al*, 2009; Fallet *et al*, 2014; Jay *et al*, 2016). Yet, evidence from mammalian cells suggest that telomeric replication intermediates require additional processing to promote telomerase access to restore telomere length and prevent

toxic structures (Margalef *et al*, 2018). In this situation, telomeric components likely modulate the access or the activity of fork remodelling factors at telomeres. Therefore, an intricate relationship exists between telomeric components, replication factors and DNA repair activities, but it remains unclear how they are coordinated.

The DNA damage tolerance (DDT) pathway is an evolutionarily conserved pathway which aids DNA replication fork bypassing DNA lesions (Branzei & Szakal, 2016; Hoege *et al*, 2002; Pfander *et al*, 2005; Ulrich, 2011). The DDT pathway involves the Rad6/Rad18 ubiquitin ligase, which senses lesions. Rad6/Rad18 mono-ubiquitylates at least one subunit of Pol30 trimer (PCNA) at K164 which recruits Rad5 and stimulates translesion synthesis by error-prone polymerases (TLS) (Gallo *et al*, 2019). However, the Rad5/Ubc13/Mms2 ubiquitin ligase can also poly-ubiquitylate mono-ubiquitinylated Pol30 at K164, leading to the so-called error-free branch of the DDT pathway which results in a homology-mediated repair using the undamaged sister chromatid as a template. This pathway likely involves repriming DNA synthesis ahead of the lesion, leaving a single stranded DNA (ssDNA) gap. In current models of post-replicative template switching, the ssDNA gap is filled when the stalled nascent strand invades the newly synthesized sister strand for use as an undamaged template (Giannattasio *et al*, 2014; Minca & Kowalski, 2010). Alternatively, fork processing and restarting requires a replication fork reversal, a step involving Rad5 ATPase activity (Shin *et al*, 2018). A series of distinct enzymatic activities such as sister cohesion, helicases, recombinases, branch migration factors, DNA syntheses, endonucleases, and resolvases are involved in error-free DTT, but the exact choreography of events is unclear. Moreover, the kinetics and access of DNA repair factors to reaction intermediates are likely regulated. For instance, the PCNA trimer can also be sumoylated at K164 to recruit the Srs2 helicase, which removes Rad51 filaments needed for homology search and strand invasion (Lehmann *et al*, 2020). In this respect, the role of Rad51 recombinase in the process has been ambiguous, cooperating with DDT factors and acting in a so-called salvage pathway of the DDT, which becomes essential when template switching is deficient.

In this work we asked whether the DDT pathway acts at telomeres to assist in their replication. We demonstrate that the helicase/ubiquitin ligase Rad5 binds to telomeres

during their replication. Senescence rates measurements made in the absence of telomerase reveal that Rad5 contributes to telomere maintenance and cell viability. The acceleration of senescence in the absence of Rad5 is suppressed by deletion of Srs2 in a Rad51-dependent manner, suggesting that Rad5 and Rad51 have partially independent activities at telomeres. Accordingly, Rad51 is exclusively recruited at short telomeres while Rad5 potentially acts at all telomeres to assist the processing of the 3'-overhang at each passage of the replication fork. Our results suggest that the reconstitution of telomeric structure could be mechanistically linked to replication stress intrinsic to telomeres.

Results

Rad5 binds to telomeres during their replication

We previously reported that the ubiquitin ligase/helicase Rad5 binds to telomeres independent of their length and is required to sustain viability of telomerase-negative budding yeast cells (Fallet *et al.*, 2014). We hypothesized that Rad5, involved in DDT pathway, participates in the replication of telomeres, helping the fork to bypass replication barriers. To test this hypothesis, we determined whether Rad5 associates with telomeres during replication using chromatin immunoprecipitation (ChIP). We blocked cells in G1, then released them and followed their progress into S-phase (Figure 1A and supplementary Figure 1A). We monitored fork passage using ChIP for replication protein A (RPA) (Waga & Stillman, 1998). Consistent with previous reports (Mattarocci *et al*, 2014), genomic regions corresponding to early and late origins fire at 45 and 60-75 min, respectively, after the release from the G1 block, while fork passage at two native telomeres (telomere 6R and 15L, containing a telomere-proximal subtelomeric X element and no Y' subtelomeric element) is at 90 min (Figure 1B and EV1B). We used the same ChIP samples to assess Myc-tagged Rad5 (Rad5-Myc) recruitment to telomeres. While we did not observe an enrichment of Rad5 at origins when they are fired, we did observe a Rad5 peak at the telomeres 6R and 15L at 90 min, which were absent in *rad5Δ* cells (Figure 1C and EV1C). Rad5 peaked at the same time as RPA at telomeres, suggesting that telomeres recruit additional Rad5 during replication, compared to other regions of the genome, perhaps because of their difficult replication.

Rad5 has a specific role at telomeres

Defects in telomere replication, resulting in truncated telomeres, can be restored by telomerase (Chang *et al*, 2007; Miller *et al.*, 2006). In the absence of telomerase, defects in telomere replication can lead to premature senescence, caused by the occurrence of at least one critically short telomere (Abdallah *et al.*, 2009; Ballew & Lundblad, 2013), which might explain how *RAD5* deletion results in accelerated loss of viability in the absence of telomerase (Fallet *et al.*, 2014) (see also Figure 3). To determine which functions of Rad5 are involved in telomere maintenance, we used a population cell viability assay in the absence

of telomerase to score the impact of mutations potentially affecting telomeric replication. We tested the effects of Rad5 separation-of-function mutations on senescence rates (Figure EV2A). In accordance with previous results, the Rad5-GAA, Rad5-I916A, and Rad5-AA mutations in the helicase and RING domain domains had smaller effect on UV and methyl methanesulfonate (MMS) sensitivity, compared to the full deletion of *RAD5* (Figure EV2B), indicating that, while displaying separation-of-function phenotypes in specific contexts, in cells challenged with genotoxic stresses, they behave as hypomorphs with respect to viability (Ball *et al*, 2014; Gallo *et al.*, 2019; Gangavarapu *et al*, 2006; Ortiz-Bazan *et al*, 2014). Moreover, these mutants, like the *RAD5* deletion, did not alter the telomere length (Figure EV2C). The Rad5 mutations had no effect on senescence timing in cells lacking *TLC1*, which encodes the telomerase RNA template (Singer & Gottschling, 1994) (Figure 2A-C, EV2D). Thus, helicase and ubiquitin ligase functions of Rad5 do not seem to be essential in sustaining cell growth in the absence of telomerase. We conclude that telomerase inactivation likely affects cells in a manner similar to a low dose of MMS or UV, for which Rad5 hypomorph mutations of Rad5 have little or no effect on viability. This result is in accordance with the idea that the function of the full length Rad5 in replication is more important than the helicase or ubiquitin ligase biochemical activities taken separately, because Rad5 is also required for the recruitment of TLS polymerases (Gallo *et al.*, 2019).

Given that Rad5 plays a major role in DDT, we asked whether other DDT components are involved in telomere maintenance, using the same senescence assays (Figure EV2E). Deletion of TLS polymerase subunits Rev1, Rev3 (polymerase zeta), or Rad30 (polymerase eta) did not accelerate senescence (Figure 2D and EVF-G). To understand the role of Pol30-K164 poly-ubiquitylation in telomere maintenance, we deleted *MMS2* and *UBC13*, which encode the other subunits of ubiquitin-conjugating enzyme complex (E2) that cooperates with Rad5, and observed a significantly loss in cell viability upon challenge with UV or MMS, however, the effect was not as severe as for *RAD5* deletion (Figure EV2B). *mms2*Δ and *ubc13*Δ cells did not accelerate senescence in *tlc1*Δ cells (Figure 2E-F), confirming previous observations in *tlc1*Δ *mms2*Δ cells with native telomeres of wild-type length (Fallet *et al.*, 2014). Given that PCNA can also be ubiquitylated on lysine K107 by Rad5 and Mms2 acting with the E2 ligase, Ubc4 (Das-Bradoo *et al*, 2010) we asked whether other E2 ubiquitin

ligases might function together with Rad5 at telomeres. However, neither *UBC4* deletion or *pol30-K107R* mutation accelerated the onset of senescence (Figure EV2H-J). Therefore, the mechanism of Rad5 telomere protection does not seem to rely on Ubc4 or Pol30-K107 mono-ubiquitylation. Thus, the complete loss of *RAD5* had largest effect on viability compared to the other DDT factors tested.

Rad5 and Rad51 have partially additive roles in the absence of telomerase

Rad51 also functions in the error-free DDT pathway, possibly contributing to strand invasion and annealing of parental strands at fork junctions or at ssDNA gaps (Branzei & Szakal, 2017; Liberi *et al*, 2005). However, in budding yeast, Rad51 activity at replicative forks is restrained by the helicase Srs2 to prevent Rad51-dependent recombination, potentially leading to gross chromosomal rearrangements. In turn, Srs2 is recruited to forks by the sumoylation of PCNA, principally at lysine 164 (Hoege *et al.*, 2002) (Figure EV2E). *SRS2* deletion suppresses genotoxic sensitivity caused by *RAD5* deletion (Broomfield & Xiao, 2002; Friedl *et al*, 2001; Ulrich, 2001). Rad51 is critical for viability of cells in which telomerase is inactivated (Ballew & Lundblad, 2013; Fallet *et al.*, 2014; Le *et al*, 1999; Lundblad & Blackburn, 1993). While its role in post-senescence survival and inter-telomeric recombination is well established, the function of Rad51 at telomeres early during telomerase inactivation is unclear (Ballew & Lundblad, 2013; Xu *et al*, 2015).

We thus asked whether Rad51 contributes to telomere maintenance through its role in DDT. To test this idea, we checked whether the genetic interactions between *rad5Δ, srs2Δ,* and *pol30–K164R* mutations seen during genotoxic exposure were recapitulated in the absence of telomerase. Prior to this, we checked that *pol30-K164R* conferred UV sensitivity to WT cells at a level similar to *rad5Δ*, and the *rad5Δ pol30-K164R* double mutant was nearly epistatic to *rad5Δ* (Figure EV3A). In contrast, *srs2Δ* only mildly affected cells exposed to UV, but completely suppressed *rad5Δ* defects in *srs2Δ rad5Δ* . These results are consistent with the current model of DDT. Indeed, both the Pol30-K164 ubiquitylation-dependent error-prone, and Rad5-dependent error-free pathways are required for full cell viability upon genotoxic exposure, whereas *SRS2* deletion allows unrestrained Rad51 action, compensating for Rad5 inactivation (Figure EV2E).

However, *pol30-K164R* had no effect on cell viability in the absence of telomerase, in contrast to UV exposure, and only slightly alleviated the effect of *RAD5* deletion (Figure 3A). *SRS2* deletion suppressed *RAD5* deletion (Figure 3B), as seen with UV exposure. This suggests that sumoylation of PCNA and recruitment of Srs2 have a role at telomeres. The *srs2-ΔSIM* (Miura *et al*, 2013) mutant, which lacks the C-terminal portion of Srs2 containing both the PCNA interaction motif (PIP) and a SUMO-interaction motif (SIM), also suppressed the phenotype of *rad5Δ* (Figure 3C and Figure EV3B). *srs2Δ* suppression of *rad5Δ* defects rely on *RAD51*, since *tlc1Δ rad5Δ srs2Δ rad51Δ* cells grew extremely poorly (Figure 3D). These data support the idea that PCNA sumoylation and Srs2 recruitment repress Rad51 activity. Furthermore, *rad5Δ* and *rad51Δ* had additive effects in the *tlc1Δ* background, despite the presence of Srs2 (Figure 3D). Thus, Rad51 is likely to play a critical role at telomeres in *rad5Δ* cells when not inhibited by Srs2. However, Rad5 and Rad51 may act on two partially non-overlapping pathways at telomeres, independently of Srs2, as well. For instance, telomeres in *rad5Δ* cells may become appropriate substrates of Rad51, even in the presence of Srs2 (see below).

Srs2 limits Rad51 recruitment to critically short telomeres.

Our genetic data suggest Rad51 is prevented from rescuing defects at telomeres in *rad5Δ* cells by the action of Srs2. We thus asked whether Rad51 recruitment to telomeres depends on Rad5 and/or Srs2, using ChIP. Because Rad51 is detected only at critically short telomeres (Fallet *et al*., 2014), we engineered our strains to stably harbour an inducible very short telomere (Diede & Gottschling, 1999; Ribeyre & Shore, 2012). A chromosome end containing 80 bp (TG80, critically short) or 250 bp (TG250, control length telomeres) of telomeric repeats was generated *de novo* upon incubation of cells in media containing galactose (Figure 4A and EV4A). We also inhibited telomerase, which would otherwise re-elongate the newly generated critically short telomere (Diede & Gottschling, 1999) by expressing *TLC1* under the control of a P_{TetO2} promoter, repressible by addition of doxycycline (Bah *et al*, 2011). These constructs were combined in strains containing *RAD5* and *SRS2* deletions and ChIP experiments were performed using an anti-Rad51 antibody.

Only critically short telomeres (TG80) recruited Rad51 in the *RAD5 SRS2* background, whereas normal length telomeres (TG250), or a native telomeres (tel6R) in the same cells did not (Figure 4B and EV4B), consistent with previous results (Fallet *et al.*, 2014). Binding of Rad51 to TG80 increased in the absence of either *RAD5* or *SRS2*, indicating that the presence of both is required to fully prevent Rad51 recruitment to short telomeres. This is consistent with our hypothesis that telomeres in *rad5Δ* cells may become substrates of Rad51, even in the presence of Srs2, which only partially represses Rad51 recruitment. In the absence of both *RAD5* and *SRS2*, binding of Rad51 to TG80 further increased, compared to *rad5Δ* cells, but was not significantly different from the binding seen in *srs2Δ* cells (Figure 4B and EV4B). This suggests that Rad5 and Srs2 exert redundant, partially independent activities in preventing Rad51 accumulation at telomeres, with Srs2 exerting the greatest effect. In the same cells, a native telomere (tel6R) did not bind Rad51, in any of the mutants. We did not see accumulation of Rad51 at normal length telomeres in cells containing the TG250 telomere either, even in *srs2Δ rad5Δ* cells. We conclude that normal length functional telomeres are not substrates for Rad51, even in the absence of Srs2. This is in contrast to Rad5 and Srs2, both of which are recruited to telomeres, mostly independently of their length (Figure 4C-D and EV4C-D). These results are consistent with a model in which Rad5 is constitutively active at telomeres, whereas Rad51 only binds when telomeres become critically short. At these telomeres, Rad51's recruitment is partially restrained by Srs2 helicase activity.

Rad5 is required for telomeric 3'-overhang reconstitution

Given that Rad5 is bound to telomeres independently of their length, as well as only during replication, we hypothesized that Rad5 may be involved in telomere processing during replication fork passage, and specifically in the reconstitution of the 3'-overhang in S-phase. We synchronized cells in G1, released them into S-phase (Figure 1), prepared DNA samples, and assessed the end structure of the telomeres by restriction digestion, electrophoresis, and detection of telomeric G-strand ssDNA by direct in-gel hybridization using radio-labelled oligo $C_{1\text{-}3}A$-rich probe (Dionne & Wellinger, 1996; Wellinger *et al*, 1992). Signal obtained under such native conditions is attributed to 5' end processing of telomeres associated with the passage of the replication fork.

RAD5-MYC cells displayed a rapid increase in overhang signal during S-phase, followed by a slow decrease, as expected (Wellinger *et al.*, 1993) (Figures 5A-C, EV5A-C and EV5G-H). For telomeres that contained a terminal Y' subtelomeric element (nearly half telomeres in our strains - https://www.le.ac.uk/colleges/medbiopsych/research/gact/resources/yeast-telomeres) and migrated altogether in the gel, providing a strong signal, the signal rapidly increased at 45 min and slowly decreased until 90 min upon release from G1 block. In contrast, *rad5Δ* cells showed only a moderate increase in overhang signal, corresponding to nearly half of that seen in wild-type cells, indicating that either the extent of 5'-resection is decreased, or that it happens in only a fraction of telomeres, or it is delayed in time. We conclude that Rad5 is involved in the proper processing of telomeres at the time of their replication. Our ability to analyze S-phase at high temporal resolution allowed us to identify a delayed ssDNA telomeric signal displaying intense bands, starting at 75 min after release from G1 block. This signal could correspond to some telomeres not containing a Y' subtelomeric element (X-only telomeres) (Figure EV5G-J). This is consistent with the notion that different telomeres replicate and process their ends at different times throughout S-phase, as previously suggested (Raghuraman *et al*, 2001). Thus, the identification of Rad5 binding at telomeres at 90 min after release into S-phase at the two native X-only telomeres tel6R and 15L (Figure 1C and EV1C) is compatible with Rad5 being required for appropriate telomere maturation at the time of telomere replication.

To determine if the decrease in telomeric overhang signal is linked to the accelerated senescence seen in *rad5Δ* cells, we tested if the decrease is suppressed by *SRS2* deletion, given that *SRS2* deletion suppresses the acceleration of senescence of *rad5Δ* (Figure 3B). However, *rad5Δ srs2Δ* cells showed a similar decrease in telomere overhang signal as *rad5Δ* cells, despite growing to *RAD5 SRS2* levels in the absence of telomerase (Figure 5D-F, EV5D-F and EV5I-J). Thus, the telomere processing defect displayed by *rad5Δ* cells is a new function of Rad5, distinct from the one in the absence of telomerase.

Discussion

In this work we demonstrate that Rad5, a component of the DNA damage tolerance pathway, associates with telomeres during replication and is involved in the processing that reconstitutes the telomeric overhang. However, this role appears to be genetically independent of its role in sustaining growth in the absence of telomerase. In telomerase-negative cells, the impact of *RAD5* deletion on growth can be compensated by the action of Rad51, which is itself restrained by Srs2. However, Rad51 can be detected at telomeres only when they reach a short length, whereas Rad5 is present at telomeres independently of their length. This suggests that Rad5 and Rad51 contribute to at least two partially distinct pathways at telomeres.

Our findings indicate that the telomere processing defect in *rad5Δ* cells is unlikely to cause the increased lethality seen in the absence of telomerase because loss of Rad5 is not suppressed by *SRS2* deletion, despite *srs2Δ* suppressing the *rad5Δ* acceleration of senescence. However, for genes that affect cell growth when mutated, such as Rad5, where the doubling time of *rad5Δ* cultures is 1.4 greater than wild-type, (Gallo *et al.*, 2019; Johnson *et al*, 1992), it is difficult to determine their precise genetic interaction with telomerase inactivation in terms of growth. To precisely quantify the contribution of Rad5 in cell growth and senescence, we measured the consecutive cell cycle durations in single cell lineages of *rad5Δ* cells in the presence or absence of telomerase using a microfluidics system (Xu *et al.*, 2015) (Appendix Figure). In these experiments, where cells grow individually with no competition effects, the mortality rate in *rad5Δ* was measured ~6% per cell division, and the increased mortality upon telomerase inactivation seems to result from the additivity of *rad5*Δ basal mortality and senescence mortality. Thus, the synthetic interactions we see in population assays may rely on complex competition effects occurring in long-term cultures, as it is the case of our quantitative senescence assays shown Figures 2 and 3. Therefore, one explanation for the low viability of *rad5Δ tlc1Δ* cells could be a simple additive effect between telomerase senescence mortality and *rad5Δ* growth defect. This growth defect is likely due to a constitutive role for Rad5 during normal S-phase in assisting

replication at regions other than telomeres, and most *rad5Δ* defects in preventing DNA damage are known to be suppressed by *SRS2* deletion (Friedl *et al*., 2001; Liefshitz *et al*, 1998).

In the same vein, we can also envisage that Rad5 and Rad51 promote cell growth in the absence of telomerase in different cells with different telomere contents, and there may be no interaction between these two pathways at the molecular level. In highly heterogeneous senescent cell cultures, some cells may display critically short telomeres early after telomerase inactivation and require Rad51 for viability, whereas others may require Rad5 for independent reasons. Cells requiring Rad51 would promote homology-dependent repair at these short telomeres, in response to extended 5'-3' resection of short telomeres (Fallet *et al*., 2014). However, while in this work, we cannot identify a specific molecular defect in *rad5Δ* that explains its potential synthetic lethality with telomerase inactivation detected in long-term cultures, at this point, we cannot exclude Rad5 or the DTT pathway being involved in Rad51-dependent processing of short telomeres. PCNA-dependent Srs2 limits Rad51 binding to short telomeres (Figure 4 and EV4) and *mms2Δ* accelerates senescence of *tlc1Δ* cells specifically when a very short telomere is artificially generated (Fallet *et al*., 2014). While the role of Rad5 and Rad51 in template switching and/or replication fork structures is not well understood (Branzei & Szakal, 2016), we observed that Rad5 by itself was not required for Rad51 binding to short telomeres. Instead, short telomeres in *rad5Δ* cells are bound by more Rad51 (Figure 4 and EV4), which may be due to defective end processing of telomeres (Figure 5, EV5).

We show that Rad5 acts in telomere processing. Nearly half of the increase in overhang signal detected in S-phase at telomeres is lost in the absence of Rad5. This could be due to a reduction in resection extension, or a decrease in the fraction of telomeres being resected, or even to a delayed and less synchronized maturation of telomeres. Signal detected in the in-gel experiments is also reduced by ~50% in a *mre11Δ* background, a mutation strongly affecting the generation of the 3' telomeric overhang (Larrivee *et al*, 2004). Rad5 could be in the same pathway as Mre11, with respect to telomere processing. The Mre11 pathway involves Mre11-Rad50-Xrs2 complex nucleolytic activity, Sae2, Exo1,

and Sgs1-Dna2, and most models suggest this pathway acts on linear telomeric molecules, similarly to double-strand break processing (Bonetti *et al*, 2013; Oh & Symington, 2018). Given that Rad5 and its mammalian ortholog can promote replication fork reversal *in vitro,* and X-shaped replication intermediates *in vivo* (Achar *et al*, 2015; Bai *et al*, 2020; Kile *et al*, 2015; Minca & Kowalski, 2010; Shin *et al*., 2018), we suggest that these nuclease activities at telomeres may occur during replication fork passage and in the context of a reversed fork. Replication fork remodelling at telomeres may arise from telomeric secondary structures causing a replication fork block, or simply due to the vicinity of the termini (Doksani *et al*, 2009), raising the possibility of a conformational step in telomere processing.

Materials and Methods

Yeast strains

All strains used in this work are in a W303 *RAD5 ADE2* background (Appendix Table 1). Gene deletions and epitope-tagging were constructed as described (Longtine *et al*, 1998). Point mutations were constructed by a two-step strategy. First, a marker (*HIS3MX6* or *kLEU2*) was first inserted in the 3'-UTR of the target gene. Then a construct was amplified using a reverse primer downstream of the inserted marker, and a forward primer containing the desired mutation for the target gene. The PCR construct was used to transform naïve cells, and clones were selected with His or Leu dropout plates (Toulmay & Schneiter, 2006).

Cell synchronization and Flow Cytometry

The strains used were *MAT***a** *bar1*Δ, and an overnight culture of each was diluted about 10-fold into 540 ml of YPD. After 3.5 hr growth at 30°C, **α** factor (Bachem) was added to a final concentration of 10^{-7} M and cultures were incubated for 130 minutes at 30°C. For the release, cells were washed three times in H_20, then treated with nuclease-free Pronase (Millipore; 46 mg total), and placed in 540 ml YPD medium at 18°C. Samples were taken every 15 minutes for ChIP and flow cytometry analysis. Cell-cycle synchrony and release were checked by microscope. Cytometry analysis of the DNA content was performed using Ethanol-fixed cells and Sytox Green (Invitrogen) staining. Analysis was performed on the Accuri C6. Data was graphed using MATLAB.

Quantitative senescence assays

Senescence assays and their analysis were performed as previously described (Fallet *et al.*, 2014). Briefly, diploids heterozygous for the relevant genes and containing a *TLC1* deletion replaced by a *Mat***α** specific Nourseothricin (Nat) reporter (*PralphaNat*) were sporulated and germinated on Nat for selection of telomerase-negative spores. Genotypes were determined on a small portion of the colony, and 8 to 16 clones of each genotype were spotted on YPD supplemented with Nourseothricin (50,000 cells in the first spot, followed

by 10-fold serial dilutions). After 46 hours at 30°C, plates were scanned (Passage 1). Cells were then picked from the most concentrated spot, to re-spot as previously for Passage 2. Passage 3 was obtained in the same manner with cells from Passage 2. Spot intensity was measured from scans after 46 h of growth and used to determine a viability index (corresponding to the dilution required to reach a given intensity threshold) using ImageJ 1.46a. Viability indexes for each genotype were plotted as boxplots using MATLAB. p-values were determined using pairwise Wilcoxon rank-sum tests in MATLAB (*= $p < .05$; ** = $p < .005$). At least two complete and biological independent experiments using independent transformants were performed for each pair of diploid starting strains and one is shown.

Chromatin Immunoprecipitation

ChIP was performed as previously described (Mattarocci *et al.*, 2014). For each ChIP culture, 40 mL of cells (at about 1e7 cells/mL) were fixed in 1% formaldehyde for 5 minutes, then the reaction was stopped with 2 mL 2.5 M glycine. Next, cells were washed with ice cold HBS twice [HBS: 50 mM HEPES pH 7.8, 140 mM NaCl], and frozen in 600 µL of ChIP lysis buffer plus with protease inhibitors and 1 mM PMSF (Roche 11836170001) [ChIP lysis buffer: 50 mM HEPES pH 7.8, 140 mM NaCl, 1 mM EDTA, 1% NP40, 1% Sodium deoxycholate]. Cells were lysed using a FastPrep (MP Biomedicals), 3x30 seconds at 6 M/s and zirconium/silica beads (BioSpec Products 11079105z). Next, beads were removed from lysates by using a needle to poke a hole in the tube and spinning the sample into a clean tube. Supernatant and pellet were resuspended in 600 µL lysis buffer and protease inhibitors, and samples were sonicated at high setting, 30 s on 30 s off for 10 minutes using a Diagenode with continuously cooled water bath at 4°C. Sonicates were clarified by spinning top speed for 30 mins at 4°C. Immunoprecipitations were set up with either anti Myc (9E10 from hybridoma culture supernatant (gift from David Shore's lab), anti-Rad51 (Abcam ab63798), or anti-RPA (polyclonal Agrisera AS07214 directed against the three RPA subunits). After 1 hr of incubation at 4 °C with rotation with antibody, either sheep anti-mouse (Invitrogen: 11201D) or sheep anti-rabbit (Invitrogen: 11203D) beads were added and incubated for 2 hours at 4°C with rotation. For washes, samples were placed on a magnet to collect beads. Beads were first rinsed in 1 mL ChIP lysis buffer and transferred to a new tube. Then, beads

were washed with AT1, AT2, AT3, and AT4 wash buffers [AT1: 50 mM HEPES pH 7.8, 140 mM NaCl, 1mM EDTA, 0.03% SDS (added freshly); AT2: 50 mM HEPES pH 7.8, 1M NaCl, 1 mM EDTA; AT3: 20 mM Tris, 250 mM LiCl, 1 mM EDTA, 0.5% NP40, 0.5% Sodium deoxycholate; AT4: 20 mM Tris pH 7.5, 0.1 mM EDTA]. After washes, sample was eluted in 140 µL of elution buffer (AT4 + 1% SDS). Samples, including 10 µL of each input, were reverse crosslinked overnight in 140 µL elution buffer at 65°C. The next day, samples were digested in proteinaseK/TE for 1 hour at 37°C, and then cleaned-up using a QIAquick PCR Purification Kit (Qiagen 28104).

qPCR was performed in a 10 µL volume with PowerSYBR green PCR master mix (Applied Biosystems 4367659) on the Applied Biosystems. The program used for the reactions is: 95°C for 10 min, then a 44x loop of 95°C 15 sec, 60°C for 1 min. Primers are listed in Appendix Table 2. Percent input was calculated by the equation percent input = $(E)^{Ct(input)-Ct(IP)}$, where E is the PCR efficiency of the primer set. The $Ct_{(input)}$ was first corrected for dilution by the formula $Ct'=Ct - \log_E(30)$.

Southern Blotting

Southern blot analysis was performed using 250 ng of DNA from each strain. DNA was digested with *Xho* I, separated on a 1.2% agarose gel, and transferred to Hybond-XL membrane. The blots were probed with a 1 kb probe for Y'-prime elements. The primers used to make the probe were Fwd: 5'- GAGTTTTTCAGCGTTTGCGTTCCA-3' Rev: 5'-TTACTCTCGCTGTCACTCCTTACC-3'. The membranes were hybridized in Church buffer at 65°C overnight, and washed four times in Church wash buffer [Church buffer: 500 mM sodium phosphate pH 7.4, 1 mM EDTA; 7% SDS, 1% BSA; Church wash buffer: 20 mM sodium phosphate pH 7.4, 1 mM EDTA, 1% SDS].

In-gel hybridization

DNA was extracted from cells lysed with glass beads in [2% Triton X-100, 1% SDS, 100 mM NaCl, 1 mM EDTA, 10 mM Tris (pH 8)], followed by a phenol-chloroform extraction and precipitation with Ethanol. Pellet was resuspended in TE with RNAse A, incubated at 37°C

for 30 minutes and re-precipitated with Ethanol. Samples were never vortexed or heated throughout the process. 500 ng of each sample was digested overnight with *Xho* I and run on a 0.7% SeaKem Agarose (Lonza) gel in 1xTBE, at 23 volts for 18-19 hours (125 mL gel, 15x15 cm). The gel was stained with ethidium bromide after running for picture. Next, the gel was dried in a gel dryer without heat, and hybridized overnight at 37°C in a sealed bag without shaking. For the hybridization, probe was mixed in 25 mL of Denhardt's hybridization solution [5xSSC, 0.5 mM Ppi, 1 mM Na_2HPO_4, 5x Denhardt's solution (Sigma Aldrich D2532), 40 nM ATP, 20 µg µg denatured salmon sperm DNA] for both native and denatured gels. Probe was prepared incubating 200 ng of oligo oT1135 (5'-CACACCCACACACCACACCCA-3') with 5 µL of γ-[^{32}P]-ATP and 1 U of T4 polynucleotide kinase (PNK, Biolabs) in buffer recommended by manufacturer 1h at 37°C, followed by 15 min at 68°C and purification using an Illustra Microspin G-25 column. The native gel was washed in 0.25x SSC, then exposed to a phosphor screen before denaturing. For denaturing, the gel was soaked in 500 mL denaturing solution [150 mM NaCl, 0.5 M NaOH] for 25 mins at room temp without shaking. Then, incubated in 200 mL neutralization solution [150 mM NaCl, 0.5 M Tris pH8] for 20 mins with shaking. The denatured gel was then hybridized in the same manner as the native gel, with freshly labeled probe. After hybridization, the denatured gel was washed in 0.1x SSC and exposed. Results were analysed with a Typhoon FLA9500 and quantified with ImageQuant TL 8.2.

Acknowledgements

We wish to thank D. Shore, M. Lisby, G. Charvin, E. Bonnel and R. Wellinger for sharing strains, reagents and technical advice and G. Riddihough from Life Science Editors for help editing the manuscript. We also thank the Teixeira lab and of the UMR8226 unit members for technical support and fruitful discussions. Work in MTT lab was supported by the European Research Council (ERC- 2010-StG 260906—D-END), the Mairie de Paris (Programme Emergences), the "Fondation de la Recherche Medicale" ("équipe labellisée") and by the French National Research Agency (ANR) as part of the "Investissements d'Avenir" Program (LabEx Dynamo ANR-11-LABX-0011-01) and ANR-16-CE12-0026. EH was supported by a fellowship from the Ligue Contre le Cancer (France). ZX is supported by ANR grant ANR-17-CE20-0002-01 and Mairie de Paris (Programme Emergences).

Conflict of Interest

The authors declare no conflict of interest

References

Abdallah P, Luciano P, Runge KW, Lisby M, Geli V, Gilson E, Teixeira MT (2009) A two-step model for senescence triggered by a single critically short telomere. *Nat Cell Biol* 11: 988-993

Achar YJ, Balogh D, Neculai D, Juhasz S, Morocz M, Gali H, Dhe-Paganon S, Venclovas C, Haracska L (2015) Human HLTF mediates postreplication repair by its HIRAN domain-dependent replication fork remodelling. *Nucleic Acids Res* 43: 10277-10291

Artandi SE, DePinho RA (2000) A critical role for telomeres in suppressing and facilitating carcinogenesis. *Current opinion in genetics & development* 10: 39-46

Bah A, Gilson E, Wellinger RJ (2011) Telomerase is required to protect chromosomes with vertebrate-type T2AG3 3' ends in Saccharomyces cerevisiae. *The Journal of biological chemistry* 286: 27132-27138

Bai G, Kermi C, Stoy H, Schiltz CJ, Bacal J, Zaino AM, Hadden MK, Eichman BF, Lopes M, Cimprich KA (2020) HLTF Promotes Fork Reversal, Limiting Replication Stress Resistance and Preventing Multiple Mechanisms of Unrestrained DNA Synthesis. *Mol Cell*

Ball LG, Xu X, Blackwell S, Hanna MD, Lambrecht AD, Xiao W (2014) The Rad5 helicase activity is dispensable for error-free DNA post-replication repair. *DNA Repair (Amst)* 16C: 74-83

Ballew BJ, Lundblad V (2013) Multiple genetic pathways regulate replicative senescence in telomerase-deficient yeast. *Aging Cell*

Bonetti D, Martina M, Falcettoni M, Longhese MP (2013) Telomere-end processing: mechanisms and regulation. *Chromosoma*

Branzei D, Szakal B (2016) DNA damage tolerance by recombination: Molecular pathways and DNA structures. *DNA Repair (Amst)* 44: 68-75

Branzei D, Szakal B (2017) Building up and breaking down: mechanisms controlling recombination during replication. *Crit Rev Biochem Mol Biol* 52: 381-394

Broomfield S, Xiao W (2002) Suppression of genetic defects within the RAD6 pathway by srs2 is specific for error-free post-replication repair but not for damage-induced mutagenesis. *Nucleic Acids Res* 30: 732-739

Campisi J, d'Adda dFF (2007) Cellular senescence: when bad things happen to good cells. *Nat Rev Mol Cell Biol* 8: 729-740

Chang M, Arneric M, Lingner J (2007) Telomerase repeat addition processivity is increased at critically short telomeres in a Tel1-dependent manner in Saccharomyces cerevisiae. *Genes Dev* 21: 2485-2494

Coutelier H, Xu Z, Morisse MC, Lhuillier-Akakpo M, Pelet S, Charvin G, Dubrana K, Teixeira MT (2018) Adaptation to DNA damage checkpoint in senescent telomerase-negative cells promotes genome instability. *Genes Dev* 32: 1499-1513

Das-Bradoo S, Nguyen HD, Bielinsky AK (2010) Damage-specific modification of PCNA. *Cell Cycle* 9: 3674-3679

Diede SJ, Gottschling DE (1999) Telomerase-mediated telomere addition in vivo requires DNA primase and DNA polymerases alpha and delta. *Cell* 99: 723-733

Diede SJ, Gottschling DE (2001) Exonuclease activity is required for sequence addition and Cdc13p loading at a de novo telomere. *Curr Biol* 11: 1336-1340.

Dionne I, Wellinger RJ (1996) Cell cycle-regulated generation of single-stranded G-rich DNA in the absence of telomerase. *Proc Natl Acad Sci U S A* 93: 13902-13907

Doksani Y, Bermejo R, Fiorani S, Haber JE, Foiani M (2009) Replicon dynamics, dormant origin firing, and terminal fork integrity after double-strand break formation. *Cell* 137: 247-258

Fallet E, Jolivet P, Soudet J, Lisby M, Gilson E, Teixeira MT (2014) Length-dependent processing of telomeres in the absence of telomerase. *Nucleic Acids Res* 42: 3648-3665

Friedl AA, Liefshitz B, Steinlauf R, Kupiec M (2001) Deletion of the SRS2 gene suppresses elevated recombination and DNA damage sensitivity in rad5 and rad18 mutants of Saccharomyces cerevisiae. *Mutat Res* 486: 137-146

Gallo D, Kim T, Szakal B, Saayman X, Narula A, Park Y, Branzei D, Zhang Z, Brown GW (2019) Rad5 Recruits Error-Prone DNA Polymerases for Mutagenic Repair of ssDNA Gaps on Undamaged Templates. *Mol Cell*

Gangavarapu V, Haracska L, Unk I, Johnson RE, Prakash S, Prakash L (2006) Mms2-Ubc13-dependent and -independent roles of Rad5 ubiquitin ligase in postreplication repair and translesion DNA synthesis in Saccharomyces cerevisiae. *Mol Cell Biol* 26: 7783-7790

Giannattasio M, Zwicky K, Follonier C, Foiani M, Lopes M, Branzei D (2014) Visualization of recombination-mediated damage bypass by template switching. *Nat Struct Mol Biol* 21: 884-892

Giraud-Panis MJ, Teixeira MT, Geli V, Gilson E (2010) CST meets shelterin to keep telomeres in check. *Mol Cell* 39: 665-676

Goto GH, Zencir S, Hirano Y, Ogi H, Ivessa A, Sugimoto K (2015) Binding of Multiple Rap1 Proteins Stimulates Chromosome Breakage Induction during DNA Replication. *PLoS Genet* 11: e1005283

Hayflick L (1965) The Limited In Vitro Lifetime Of Human Diploid Cell Strains. *Exp Cell Res* 37: 614-636

Hoege C, Pfander B, Moldovan GL, Pyrowolakis G, Jentsch S (2002) RAD6-dependent DNA repair is linked to modification of PCNA by ubiquitin and SUMO. *Nature* 419: 135-141

Ivessa AS, Zhou JQ, Schulz VP, Monson EK, Zakian VA (2002) Saccharomyces Rrm3p, a 5' to 3' DNA helicase that promotes replication fork progression through telomeric and subtelomeric DNA. *Genes Dev* 16: 1383-1396.

Jain D, Cooper JP (2010) Telomeric strategies: means to an end. *Annu Rev Genet* 44: 243-269

Jay KA, Smith DL, Blackburn EH (2016) Early Loss of Telomerase Action in Yeast Creates a Dependence on the DNA Damage Response Adaptor Proteins. *Mol Cell Biol* 36: 1908-1919

Johnson RE, Henderson ST, Petes TD, Prakash S, Bankmann M, Prakash L (1992) Saccharomyces cerevisiae RAD5-encoded DNA repair protein contains DNA helicase and zinc-binding sequence motifs and affects the stability of simple repetitive sequences in the genome. *Mol Cell Biol* 12: 3807-3818

Kile AC, Chavez DA, Bacal J, Eldirany S, Korzhnev DM, Bezsonova I, Eichman BF, Cimprich KA (2015) HLTF's Ancient HIRAN Domain Binds 3' DNA Ends to Drive Replication Fork Reversal. *Mol Cell*

Larrivee M, LeBel C, Wellinger RJ (2004) The generation of proper constitutive G-tails on yeast telomeres is dependent on the MRX complex. *Genes Dev* 18: 1391-1396

Le S, Moore JK, Haber JE, Greider CW (1999) RAD50 and RAD51 define two pathways that collaborate to maintain telomeres in the absence of telomerase. *Genetics* 152: 143-152

Lee SS, Bohrson C, Pike AM, Wheelan SJ, Greider CW (2015) ATM Kinase Is Required for Telomere Elongation in Mouse and Human Cells. *Cell Rep* 13: 1623-1632

Lehmann CP, Jiménez-Martín A, Branzei D, Tercero JA (2020) Prevention of unwanted recombination at damaged replication forks. *Curr Genet*

Liberi G, Maffioletti G, Lucca C, Chiolo I, Baryshnikova A, Cotta-Ramusino C, Lopes M, Pellicioli A, Haber JE, Foiani M (2005) Rad51-dependent DNA structures accumulate at damaged replication forks in sgs1 mutants defective in the yeast ortholog of BLM RecQ helicase. *Genes Dev* 19: 339-350

Liefshitz B, Steinlauf R, Friedl A, Eckardt-Schupp F, Kupiec M (1998) Genetic interactions between mutants of the 'error-prone' repair group of Saccharomyces cerevisiae and their effect on recombination and mutagenesis. *Mutat Res* 407: 135-145

Lingner J, Cooper JP, Cech TR (1995) Telomerase and DNA end replication: no longer a lagging strand problem? *Science* 269: 1533-1534

Longtine MS, McKenzie AI, Demarini DJ, Shah NG, Wach A, Brachat A, Philippsen P, Pringle JR (1998) Additional modules for versatile and economical PCR-based gene deletion and modification in Saccharomyces cerevisiae. *Yeast* 14: 953-961

Lue NF, Chan J, Wright WE, Hurwitz J (2014) The CDC13-STN1-TEN1 complex stimulates Pol alpha activity by promoting RNA priming and primase-to-polymerase switch. *Nat Commun* 5: 5762

Lundblad V, Blackburn EH (1993) An alternative pathway for yeast telomere maintenance rescues est1- senescence. *Cell* 73: 347-360

Makovets S, Herskowitz I, Blackburn EH (2004) Anatomy and dynamics of DNA replication fork movement in yeast telomeric regions. *Mol Cell Biol* 24: 4019-4031

Margalef P, Kotsantis P, Borel V, Bellelli R, Panier S, Boulton SJ (2018) Stabilization of Reversed Replication Forks by Telomerase Drives Telomere Catastrophe. *Cell* 172: 439-453 e414

Matmati S, Lambert S, Geli V, Coulon S (2020) Telomerase Repairs Collapsed Replication Forks at Telomeres. *Cell Rep* 30: 3312-3322.e3313

Mattarocci S, Shyian M, Lemmens L, Damay P, Altintas DM, Shi T, Bartholomew CR, Thoma NH, Hardy CF, Shore D (2014) Rif1 Controls DNA Replication Timing in Yeast through the PP1 Phosphatase Glc7. *Cell Rep* 7: 62-69

Miller KM, Rog O, Cooper JP (2006) Semi-conservative DNA replication through telomeres requires Taz1. *Nature* 440: 824-828

Minca EC, Kowalski D (2010) Multiple Rad5 activities mediate sister chromatid recombination to bypass DNA damage at stalled replication forks. *Mol Cell* 38: 649-661

Mirman Z, Lottersberger F, Takai H, Kibe T, Gong Y, Takai K, Bianchi A, Zimmermann M, Durocher D, de Lange T (2018) 53BP1-RIF1-shieldin counteracts DSB resection through CST- and Polalpha-dependent fill-in. *Nature*

Miura T, Shibata T, Kusano K (2013) Putative antirecombinase Srs2 DNA helicase promotes noncrossover homologous recombination avoiding loss of heterozygosity. *Proceedings of the National Academy of Sciences* 110: 16067-16072

Moore A, Dominska M, Greenwell P, Aksenova AY, Mirkin S, Petes T (2018) Genetic Control of Genomic Alterations Induced in Yeast by Interstitial Telomeric Sequences. *Genetics* 209: 425-438

Negrini S, Ribaud V, Bianchi A, Shore D (2007) DNA breaks are masked by multiple Rap1 binding in yeast: implications for telomere capping and telomerase regulation. *Genes Dev* 21: 292-302

Oh J, Symington LS (2018) Role of the Mre11 Complex in Preserving Genome Integrity. *Genes (Basel)* 9

Ortiz-Bazan MA, Gallo-Fernandez M, Saugar I, Jimenez-Martin A, Vazquez MV, Tercero JA (2014) Rad5 plays a major role in the cellular response to DNA damage during chromosome replication. *Cell Rep* 9: 460-468

Pfander B, Moldovan GL, Sacher M, Hoege C, Jentsch S (2005) SUMO-modified PCNA recruits Srs2 to prevent recombination during S phase. *Nature* 436: 428-433

Pfeiffer V, Crittin J, Grolimund L, Lingner J (2013) The THO complex component Thp2 counteracts telomeric R-loops and telomere shortening. *EMBO J*

Raghuraman MK, Winzeler EA, Collingwood D, Hunt S, Wodicka L, Conway A, Lockhart DJ, Davis RW, Brewer BJ, Fangman WL (2001) Replication dynamics of the yeast genome. *Science* 294: 115-121.

Ribeyre C, Shore D (2012) Anticheckpoint pathways at telomeres in yeast. *Nat Struct Mol Biol*

Sabourin M, Zakian VA (2008) ATM-like kinases and regulation of telomerase: lessons from yeast and mammals. *Trends Cell Biol* 18: 337-346

Sfeir A, Kosiyatrakul ST, Hockemeyer D, MacRae SL, Karlseder J, Schildkraut CL, de LT (2009) Mammalian telomeres resemble fragile sites and require TRF1 for efficient replication. *Cell* 138: 90-103

Shin S, Hyun K, Kim J, Hohng S (2018) ATP Binding to Rad5 Initiates Replication Fork Reversal by Inducing the Unwinding of the Leading Arm and the Formation of the Holliday Junction. *Cell Rep* 23: 1831-1839

Singer MS, Gottschling DE (1994) TLC1: template RNA component of Saccharomyces cerevisiae telomerase. *Science* 266: 404-409

Soudet J, Jolivet P, Teixeira MT (2014) Elucidation of the DNA end-replication problem in Saccharomyces cerevisiae. *Mol Cell* 53: 954-964

Stanley SE, Armanios M (2015) The short and long telomere syndromes: paired paradigms for molecular medicine. *Current opinion in genetics & development* 33: 1-9

Strecker J, Stinus S, Caballero MP, Szilard RK, Chang M, Durocher D (2017) A sharp Pif1-dependent threshold separates DNA double-strand breaks from critically short telomeres. *Elife* 6

Teixeira MT (2013) Saccharomyces cerevisiae as a Model to Study Replicative Senescence Triggered by Telomere Shortening. *Frontiers in oncology* 3: 101

Tong AS, Stern JL, Sfeir A, Kartawinata M, de Lange T, Zhu XD, Bryan TM (2015) ATM and ATR Signaling Regulate the Recruitment of Human Telomerase to Telomeres. *Cell Rep* 13: 1633-1646

Toulmay A, Schneiter R (2006) A two-step method for the introduction of single or multiple defined point mutations into the genome of Saccharomyces cerevisiae. *Yeast* 23: 825-831

Ulrich HD (2001) The srs2 suppressor of UV sensitivity acts specifically on the RAD5- and MMS2-dependent branch of the RAD6 pathway. *Nucleic Acids Res* 29: 3487-3494

Ulrich HD (2011) Timing and spacing of ubiquitin-dependent DNA damage bypass. *FEBS Lett* 585: 2861-2867

Voineagu I, Freudenreich CH, Mirkin SM (2009) Checkpoint responses to unusual structures formed by DNA repeats. *Mol Carcinog* 48: 309-318

Waga S, Stillman B (1998) The DNA replication fork in eukaryotic cells. *Annu Rev Biochem* 67: 721-751

Wellinger RJ (2014) In the end, what's the problem? *Mol Cell* 53: 855-856

Wellinger RJ, Ethier K, Labrecque P, Zakian VA (1996) Evidence for a new step in telomere maintenance. *Cell* 85: 423-433

Wellinger RJ, Wolf AJ, Zakian VA (1992) Use of non-denaturing Southern hybridization and two dimensional agarose gels to detect putative intermediates in telomere replication in Saccharomyces cerevisiae. *Chromosoma* 102: S150-156

Wellinger RJ, Wolf AJ, Zakian VA (1993) Saccharomyces telomeres acquire single-strand TG1-3 tails late in S phase. *Cell* 72: 51-60

Wellinger RJ, Zakian VA (2012) Everything You Ever Wanted to Know About Saccharomyces cerevisiae Telomeres: Beginning to End. *Genetics* 191: 1073-1105

Wu P, Takai H, de Lange T (2012) Telomeric 3' Overhangs Derive from Resection by Exo1 and Apollo and Fill-In by POT1b-Associated CST. *Cell* 150: 39-52

Xu Z, Duc KD, Holcman D, Teixeira MT (2013) The length of the shortest telomere as the major determinant of the onset of replicative senescence. *Genetics* 194: 847-857

Xu Z, Fallet E, Paoletti C, Fehrmann S, Charvin G, Teixeira MT (2015) Two routes to senescence revealed by real-time analysis of telomerase-negative single lineages. *Nature communications* 6: 7680

Zhao Y, Sfeir AJ, Zou Y, Buseman CM, Chow TT, Shay JW, Wright WE (2009) Telomere extension occurs at most chromosome ends and is uncoupled from fill-in in human cancer cells. *Cell* 138: 463-475

Figure Legends

Figure 1- Rad5 is enriched at telomeres during their replication

(A) Cells with indicated genotype were synchronized using alpha factor and released at 18°C. Timepoints were taken every 15 minutes, and analyzed by flow cytometry using Sytox Green staining to quantify DNA content (1N or 2N). (B-C) The same samples were processed for ChIP and divided in half to immunoprecipitate either RPA (B) or Rad5-Myc (C). qPCR was used to determine the amount of two individual telomeres (6R and 15L), an early ARS, (*ARS607*), and a late ARS (ARS522) bound by RPA or Rad5-Myc. Results are expressed as a percentage of the input fraction.

Figure 2- Rad5's role at telomeres does not involve helicase or ubiquitin ligase activities and is independent on the DDT pathway

(A-F) Quantitative assessment of senescence for strains with indicated genotypes. *tlc1Δ* spore-colonies derived from diploids *tlc1Δ /TLC1* combined with indicated mutations are genotyped and spotted on plates for three consecutive passages. Viability index reflects the capacity of forming colonies at each passage. Adjusted p-values were obtained by the Wilcoxon rank-sum test with a false discovery rate correction *p-value < 0.05, **p-value < 0.005.

Figure 3- Rad5- and Rad51-dependent pathways both maintain cell viability in the absence of telomerase.

(A-D) Quantitative assessment of senescence for strains with indicated genotypes. *tlc1Δ* spore-colonies derived from diploids *tlc1Δ /TLC1* combined with indicated mutations are genotyped and spotted on plates for three consecutive passages. Viability index reflects the capacity of forming colonies at each passage. Adjusted p-values were obtained by the Wilcoxon rank-sum test with a false discovery rate correction *p-value < 0.05, **p-value < 0.005.

Figure 4- Rad51 recruitment to short telomeres is prevented by Rad5 and Srs2

(A) Cells with indicated genotype grown in the presence of Dox to repress telomerase and then shifted to galactose-containing media for 4 h to generate a telomeric extremity containing 80 bp or 250 bp of telomeric repeats, were harvested and chromatin was immunoprecipitated with anti-Rad51 antibodies (B) The association of Rad51 with the newly generated telomere (TG250 or TG80) or with an internal control locus (*PDZ1*) was quantified by qPCR. An unaffected telomere (tel6R) was also assessed in the strain harboring the critically short telomere TG80 and its association with Rad51 was evaluated together with *ACT1* control locus. All data are depicted as mean + SD. p-values were obtained from two-tailed Student's t- tests (*p < 0.05, **p < 0.01). (C-D) Cells as in (A) expressing *RAD5-MYC* (C) or *SRS2-MYC* (D) grown in the presence of Dox and then shifted to galactose-containing media for 4h, were harvested and chromatin was immunoprecipitated with anti-Myc antibodies. The association of Rad5-Myc or Srs2-Myc with the newly generated telomere (TG250 or TG80) or with an control internal locus (*PDZ1*) was quantified by qPCR. An unaffected telomere (tel6R) was also assessed in the strain harboring the critically short telomere TG80 and its association with indicated proteins was evaluated in parallel to *PDZ1* control locus. All data are depicted as mean + SD. See Figure EV4 for experimental details and results in independent clones and replicates.

Figure 5- Rad5 contributes to the processing of telomeres after the passage of the replication fork

P_{TetO2}-*TLC1* cells with indicated *RAD5* and *SRS2* genotypes were synchronized using alpha factor and released at 18°C as in Figure 1. (A, D) Timepoints were taken every 15 minutes, and analysed by flow cytometry to quantify DNA content (1N or 2N). (B, E) DNA was extracted in native conditions, digested with *Xho* I, electrophoresed and hybridized in-gel with a CA-rich probe to detect the telomere 3'-overhangs (upper panels "native"). Gels were denatured and hybridized to the same probe to detect overall telomeric signal (lower panels "denatured"). Areas where Y' terminal restriction fragments migrate are shown. (C, F) Histograms representing the ratio native:denatured signals normalized to the first lane of each gel. See Figure EV5 for replicates of this experiment and raw data. Note: experiment shown in (A-C) is made out of the exact same cultures than the one in Figure 1 and EV1D-E.

Expanded View Figure Legends

Figure EV1- Rad5 localizes to telomeres during their replication

(A-C) Biological replicate of experiment shown in Figure 1A-C. (A) Cells with indicated genotype were synchronized using alpha factor and released at 18 °C. Timepoints were taken every 15 minutes, and analyzed by flow cytometry to quantify DNA content (1N or 2N). (B-C) The same samples were processed for ChIP and divided in half to immunoprecipitate either RPA (B) or Rad5-Myc (C). qPCR was used to determine the amount of two individual telomeres (6R and 15L), an early ARS, (ARS 607), and a late ARS (ARS522) bound by RPA or Rad5-Myc. Results are expressed as a percentage of the input fraction. (D-E) Similar to (A) and (C) with *rad5*Δ cells, as negative control.

Figure EV2- Effects of mutations in Rad5 and DDT components

(A) The Rad5 helicase contains a putative DNA-binding HIRAN domain (in orange), and an E3 ligase domain (blue) embedded in a SWI/SNF2 family helicase domain (green). The walker A and B motifs are depicted in dark green. (B) UV spot assays were performed with indicated *rad5* mutants. For each strain, 50,000 cells were plated in the most concentrated spot, followed by 10-fold serial dilutions. Then plates were subjected to UV at 0, 5, 10 or 25 J/m2. Plates were incubated for 48 hours. (C) Southern blot analysis was performed on various *rad5* mutants using 250 ng of DNA from each strain. DNA was digested with *Xho* I, separated on a 1.2% agarose gel, and the blot was probed with a probe for Y' elements. (D, F-J) Quantitative senescence assays were performed as in Figure 2, for indicated genotypes. * stands for *RAD5-3'-UTR::HIS3MX6* and *POL30-3'-UTR::kLEU2*. (E) Schematic of the DNA Damage Tolerance pathway (DDT) operating when replication fork encounters a DNA lesion. The DDT is initiated by the Rad6/Rad18 ubiquitin ligase, which mono-ubiquitylates Pol30 (PCNA) on K164. The mono-ubiquitylation of Pol30 stimulates error-prone translesion synthesis (TLS) by TLS polymerases (Pols), a process that involves Rad5 helicase activity. Alternatively, the E3 ligase Rad5, working with E2 ligase complex Mms2/Ubc13, poly-ubiquitylates Pol30 on K164. This poly-ubiquitylation leads to template switching, which is an error-free process assisted by Rad5 and possibly Rad51. In another branch of the

pathway, Srs2 helicase is recruited to SUMO-K164-Pol30, which blocks the activity of Rad51 by removing Rad51 filaments. Because the absence of Srs2 suppresses viability of *rad5Δ* cells, this branch is called "salvage pathway".

Figure EV3- Penetrance of DDT mutations

(A) UV spot assays were performed with indicated mutants. For each strain, 50,000 cells were plated in the most concentrated spot, followed by 10-fold serial dilutions. Then plates were subjected to UV at 0, 5, 10 or 25 J/m2. Plates were incubated for 48 hours. (B) Quantitative senescence assay as in Figure 2 for indicated genotypes. *SRS2-3'UTR-kLEU2* stands for the *SRS2* allele in which the *kLEU2* marker is inserted in the 3'UTR of *SRS2* (used to construct *srs2ΔSIM*).

Figure EV4- Individual ChIP results for Figure 4

(A) Schematic representation of the experiment to induce a *de novo* critically short telomere (TG80) or a normal length telomere (TG250). Strains in this experiment contain a unique site for HO endonuclease, flanked by a variable number of telomeric repeats. This construct is embedded within a subtelomeric region of arm 7L, containing no essential genes from there to the telomeres. Cells also contain *TLC1*, encoding for telomerase template RNA subunit, under the control of a promoter repressible by addition of doxycycline (Dox) to the media. To induce a *de novo* telomere of controlled length, cells are first pre-incubated overnight (O/N) in Dox, and then shifted for 4h into Galactose-containing media in presence of Dox, to induce the expression of endonuclease HO. This generates a new telomere containing either 250 or 80 bp of TG1-3 repeats (TG250 and TG80, respectively, depending on the strain). CEN7, centromere of chromosome 7; telomeric repeats are represented by black arrow heads, flanking markers *LYS2* and *ADE2* are depicted. (B-D) ChIP results shown in Figure 4 were obtained by averaging data shown obtained for indicated independent strains and clones (see Appendix Table 1).

Figure EV5- Replicate Ingel experiments as in Figure 5

(A-F) Legends as in Figure 5. (G-J) Full images of the gels shown in Figure 5 (G, I) and Figure EV5B, E (H, J). Migration zones of X-only telomeres and Y' telomeres are indicated.

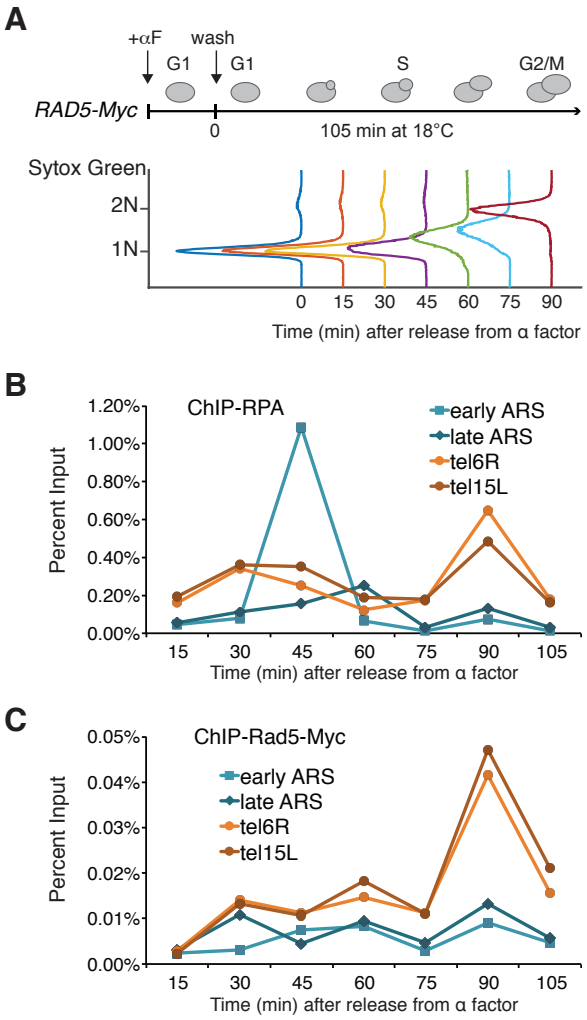

Figure 1 - Henninger et al.

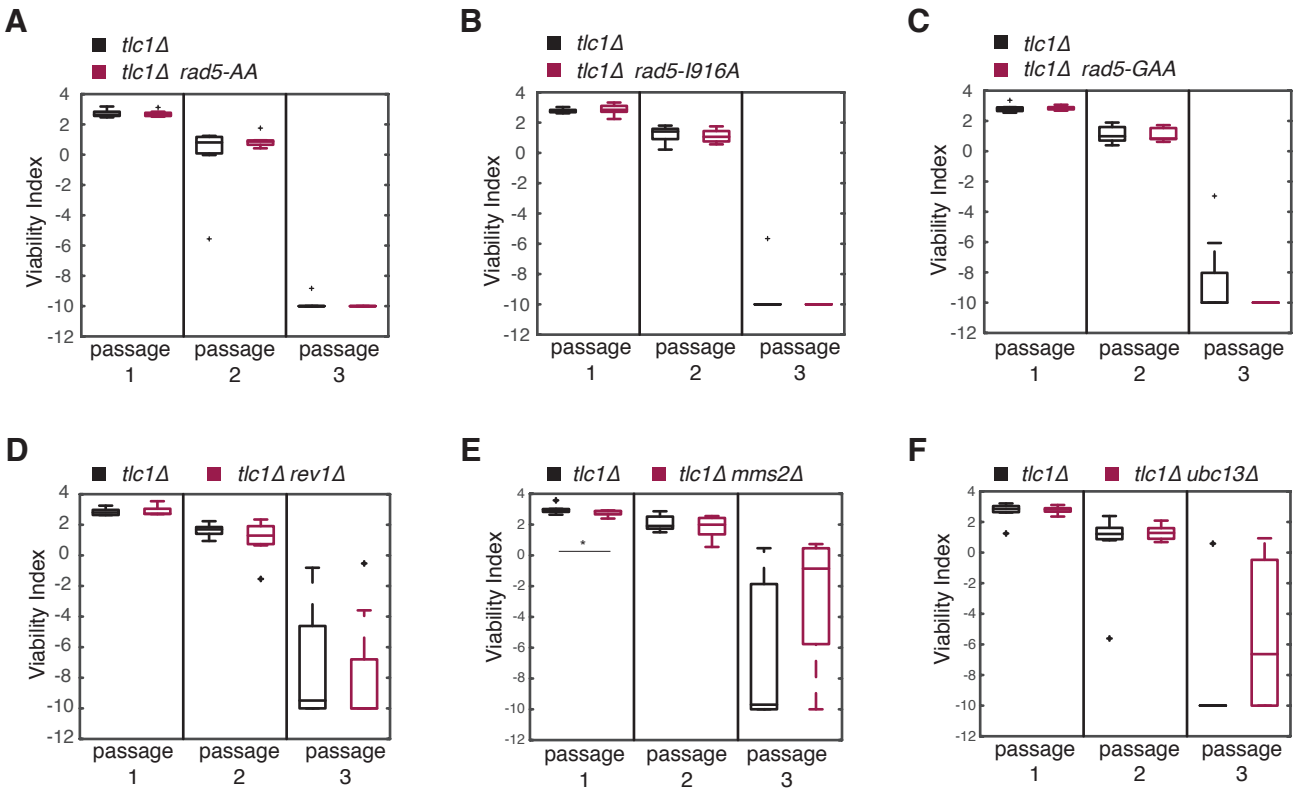

Figure 2 - Henninger et al

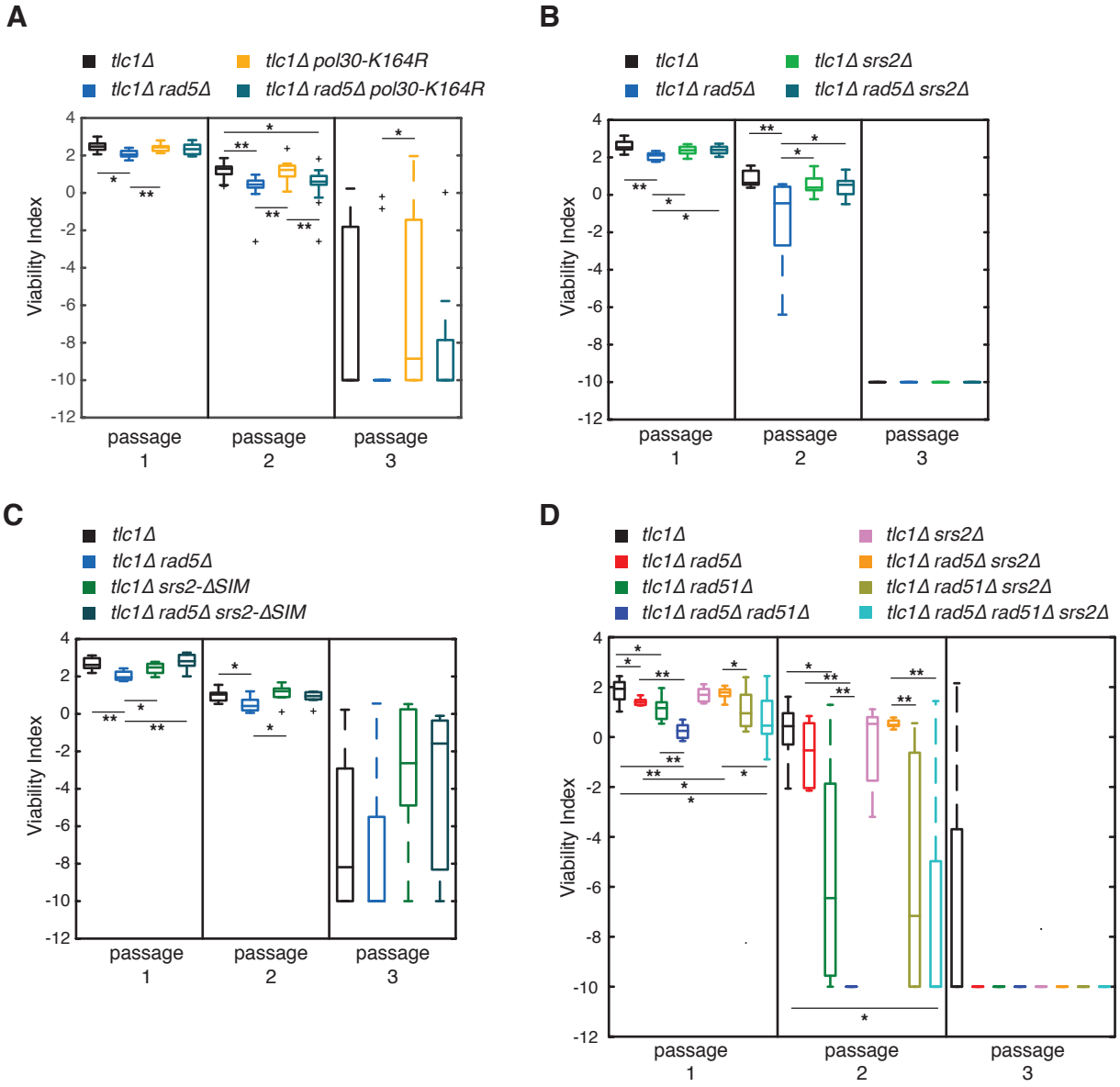

Figure 3 Henninger et al

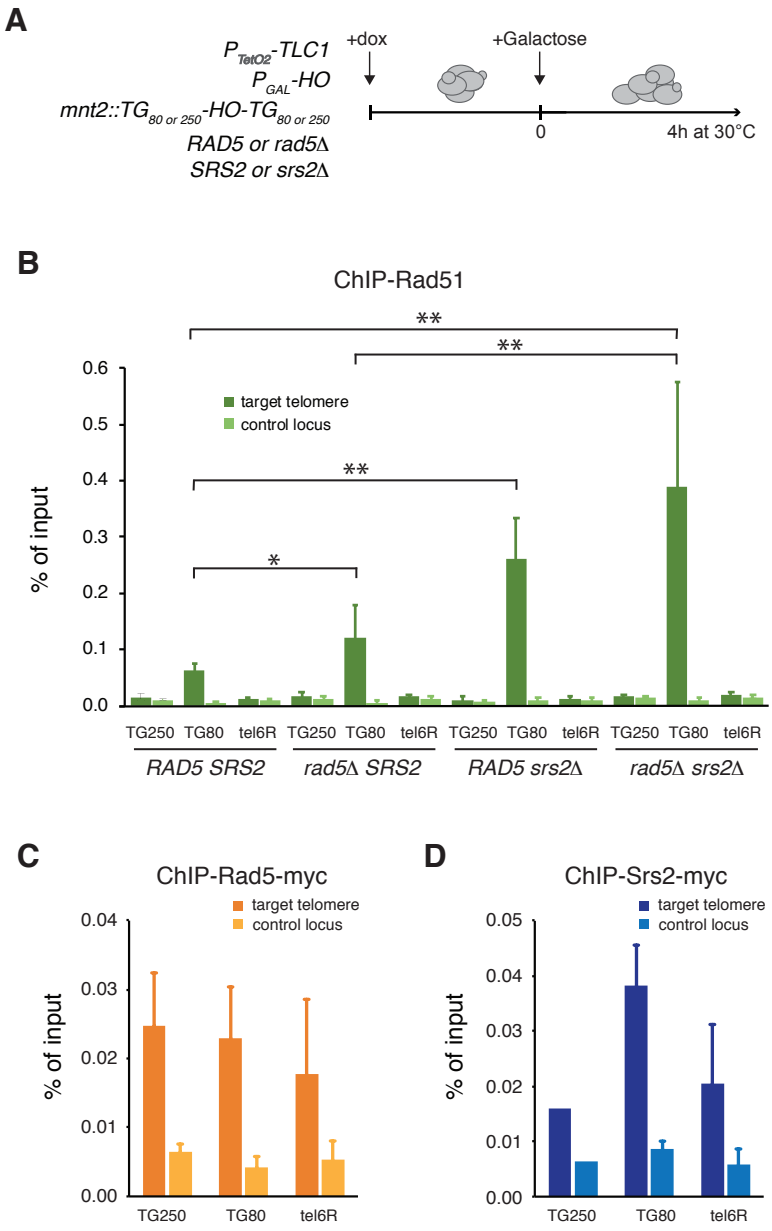

Figure 4 Henninger et al

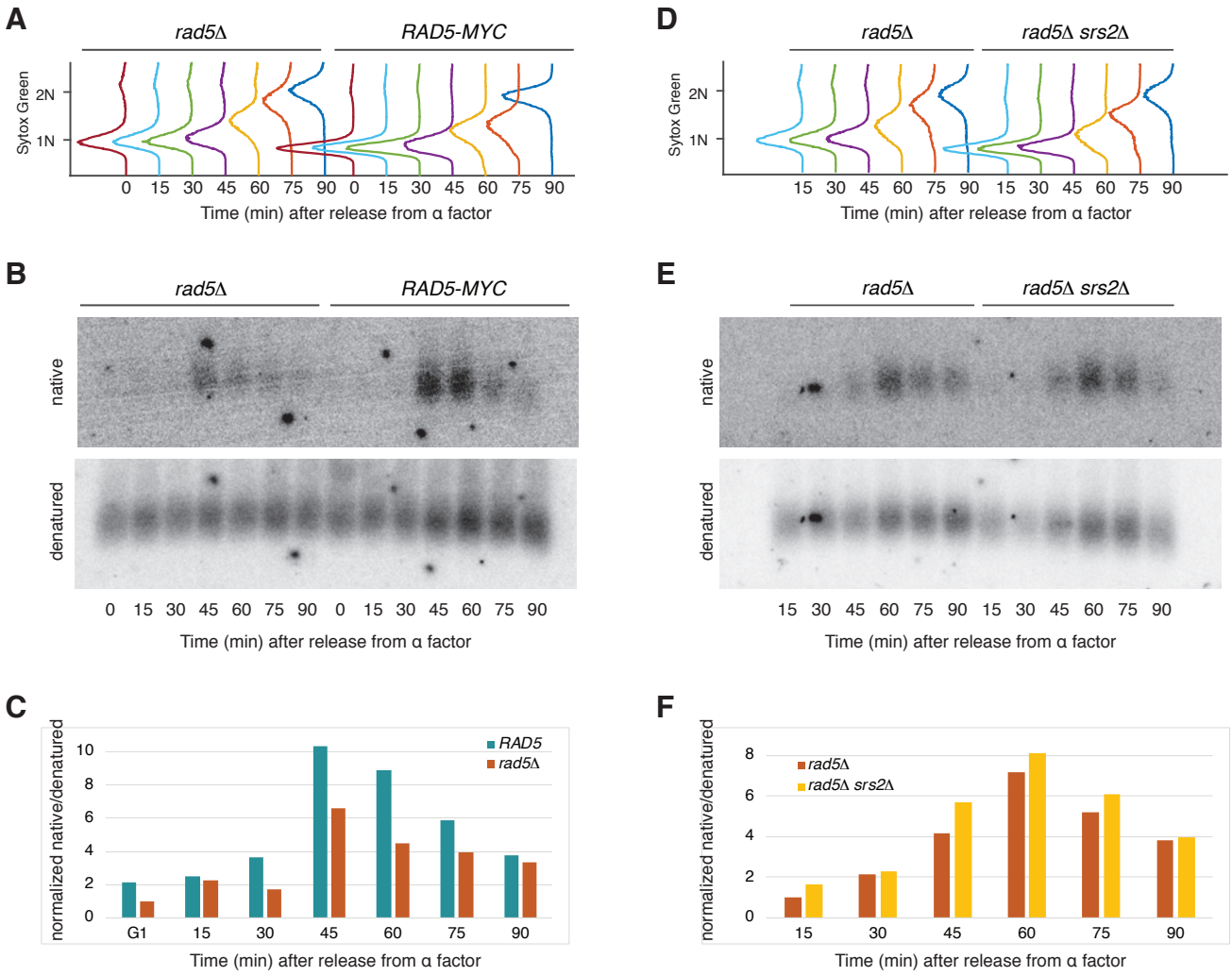

Figure 5 Henninger et al

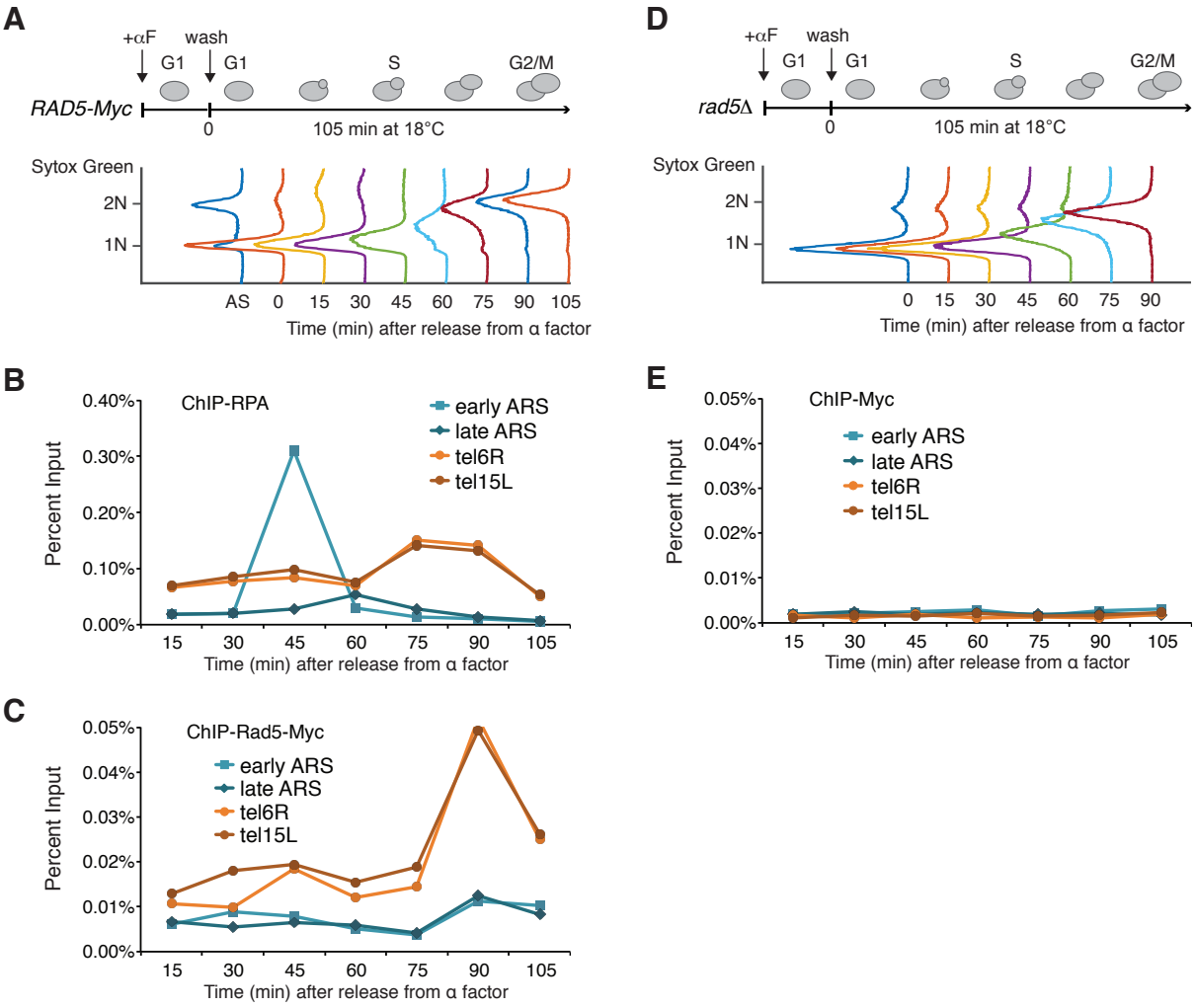

Figure EV1 - Henninger et al.

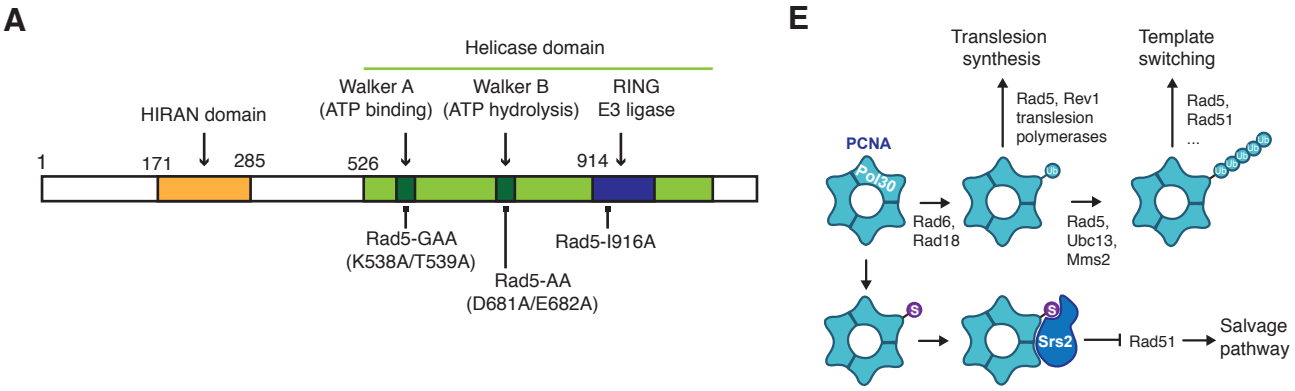

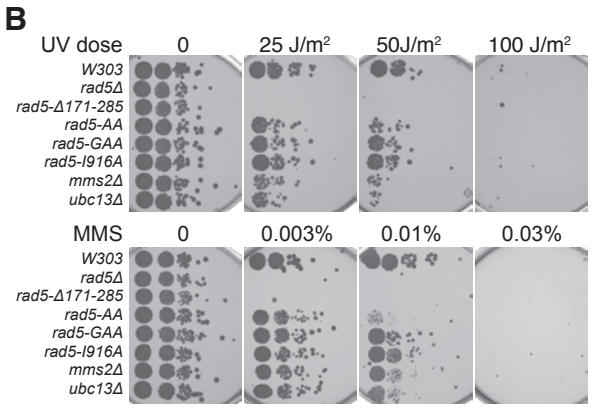

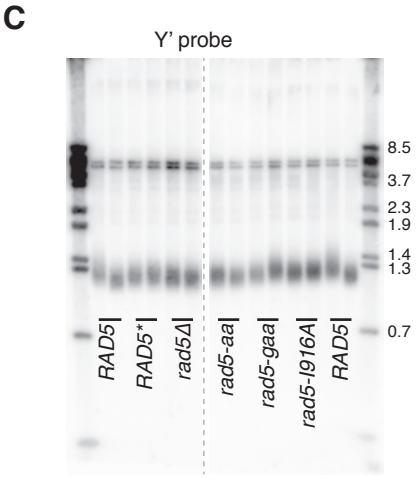

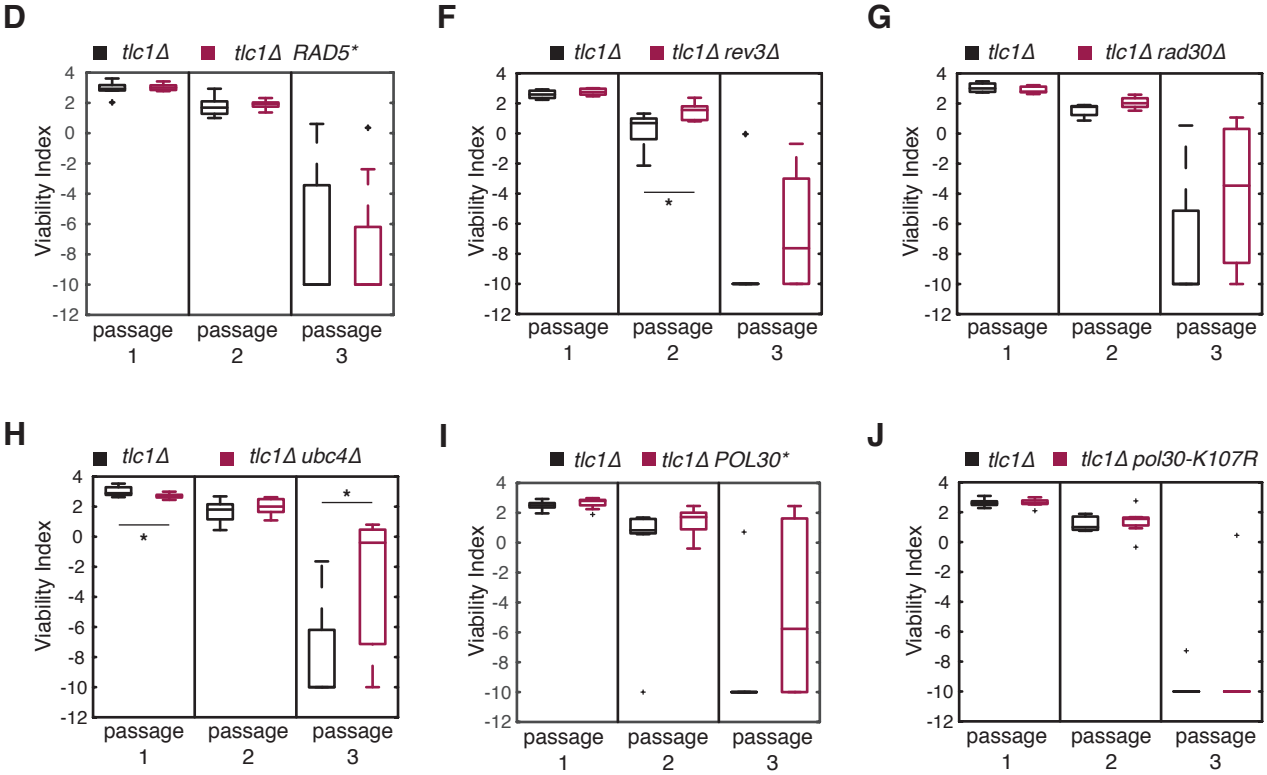

Figure EV2 - Henninger et al

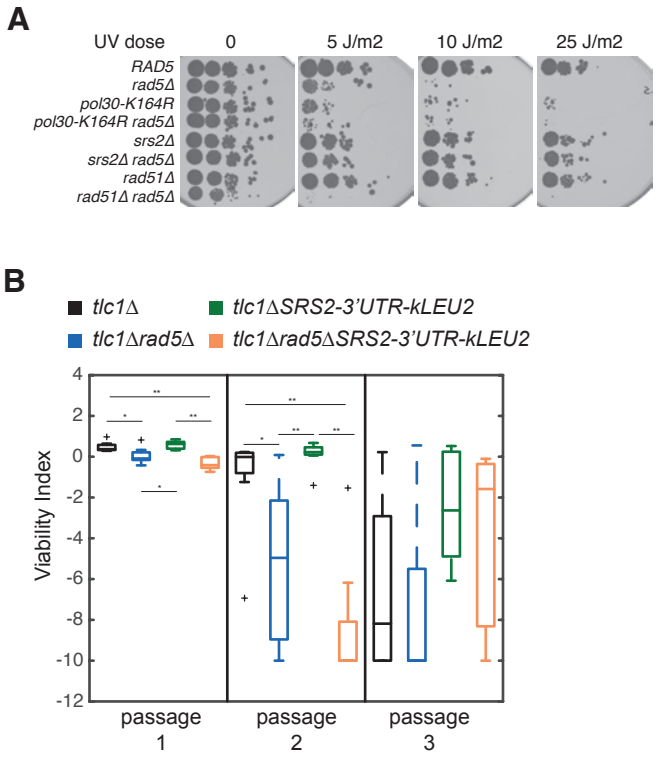

Figure EV3 - Henninger et al

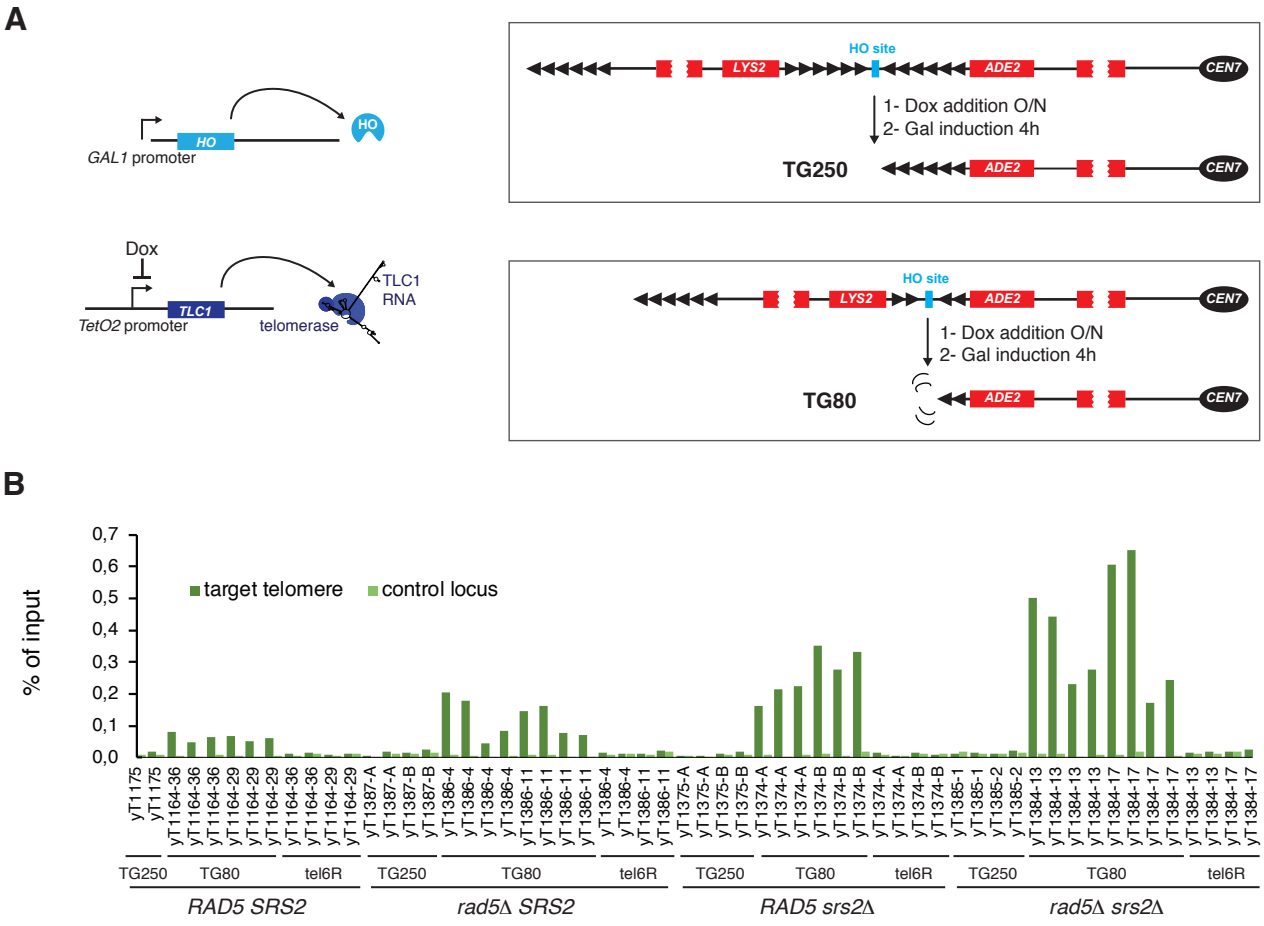

Figure EV4 - Henninger et al

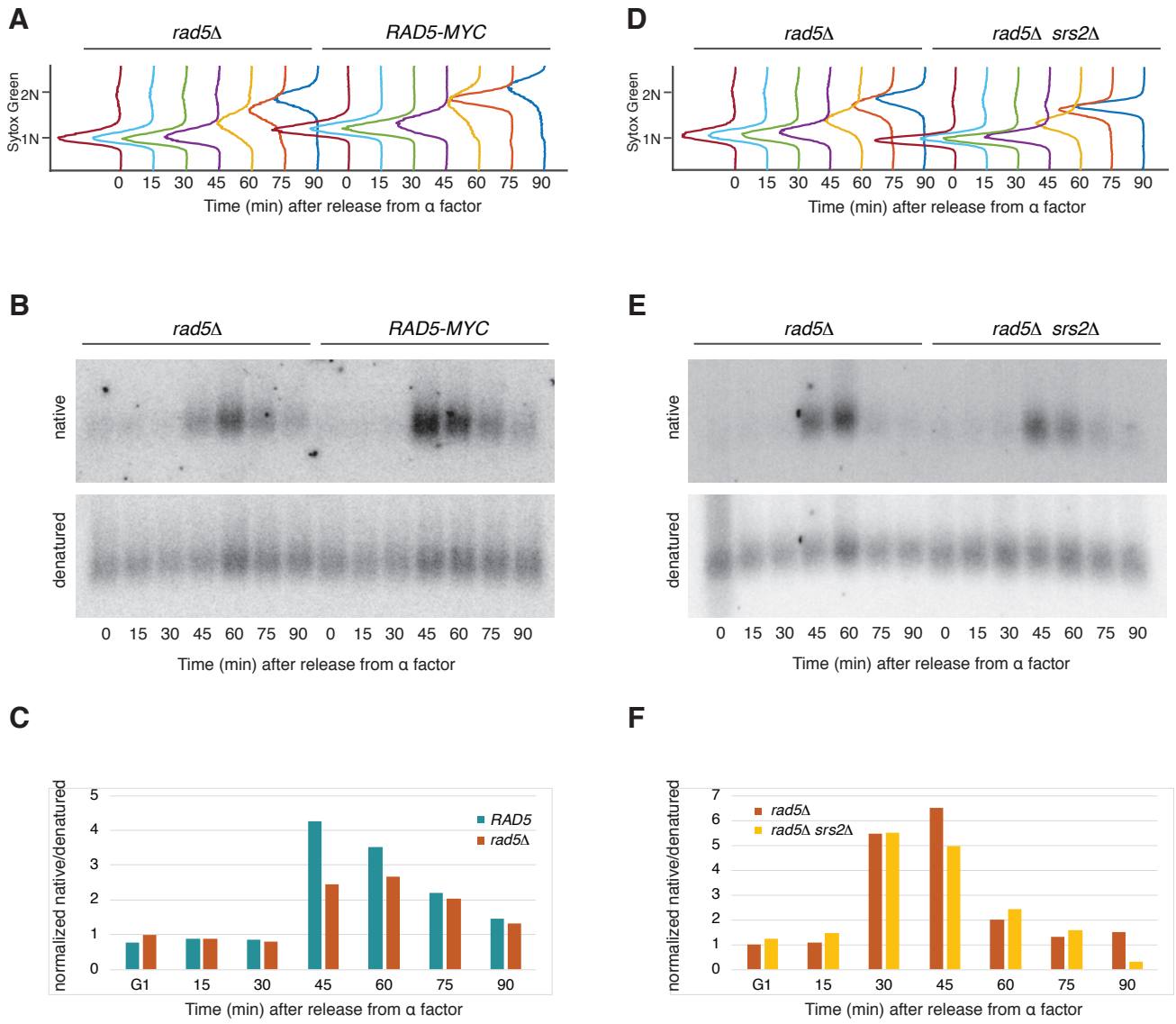

Figure EV5 - Henninger et al

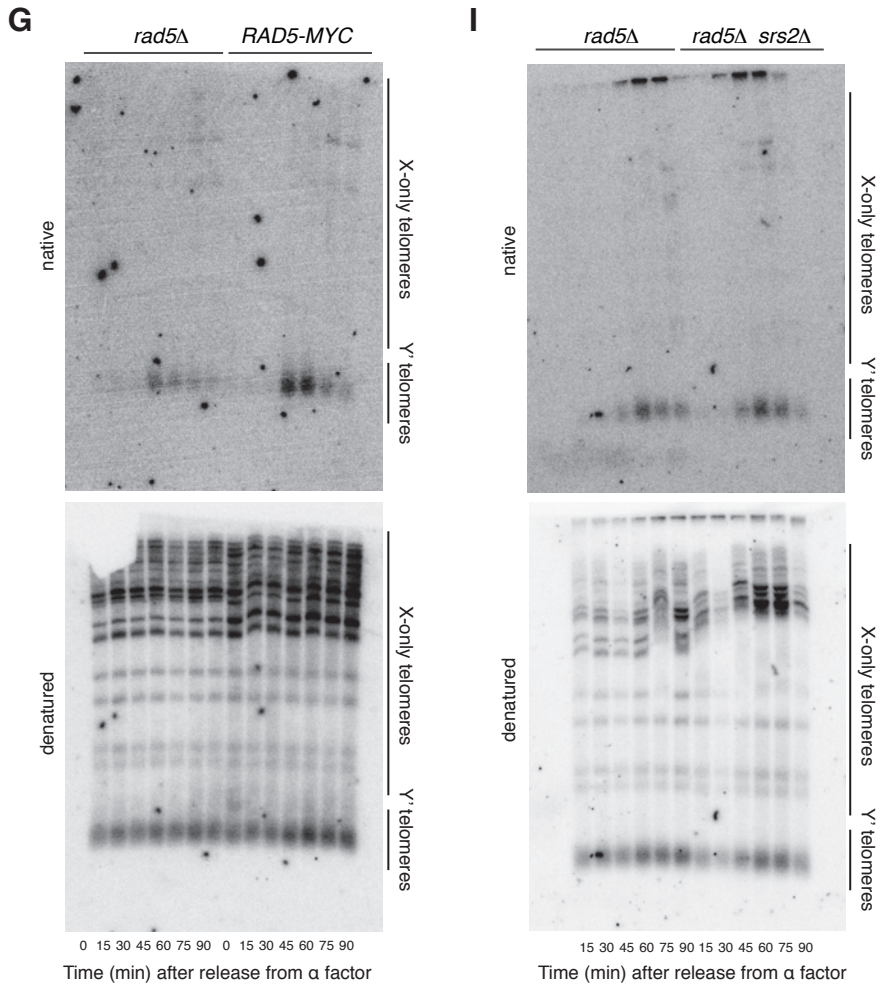

Figure EV5 - Henninger et al (continued)

Appendix related to Henninger et al.

Maturation of telomere 3'-overhangs is linked to the replication stress response

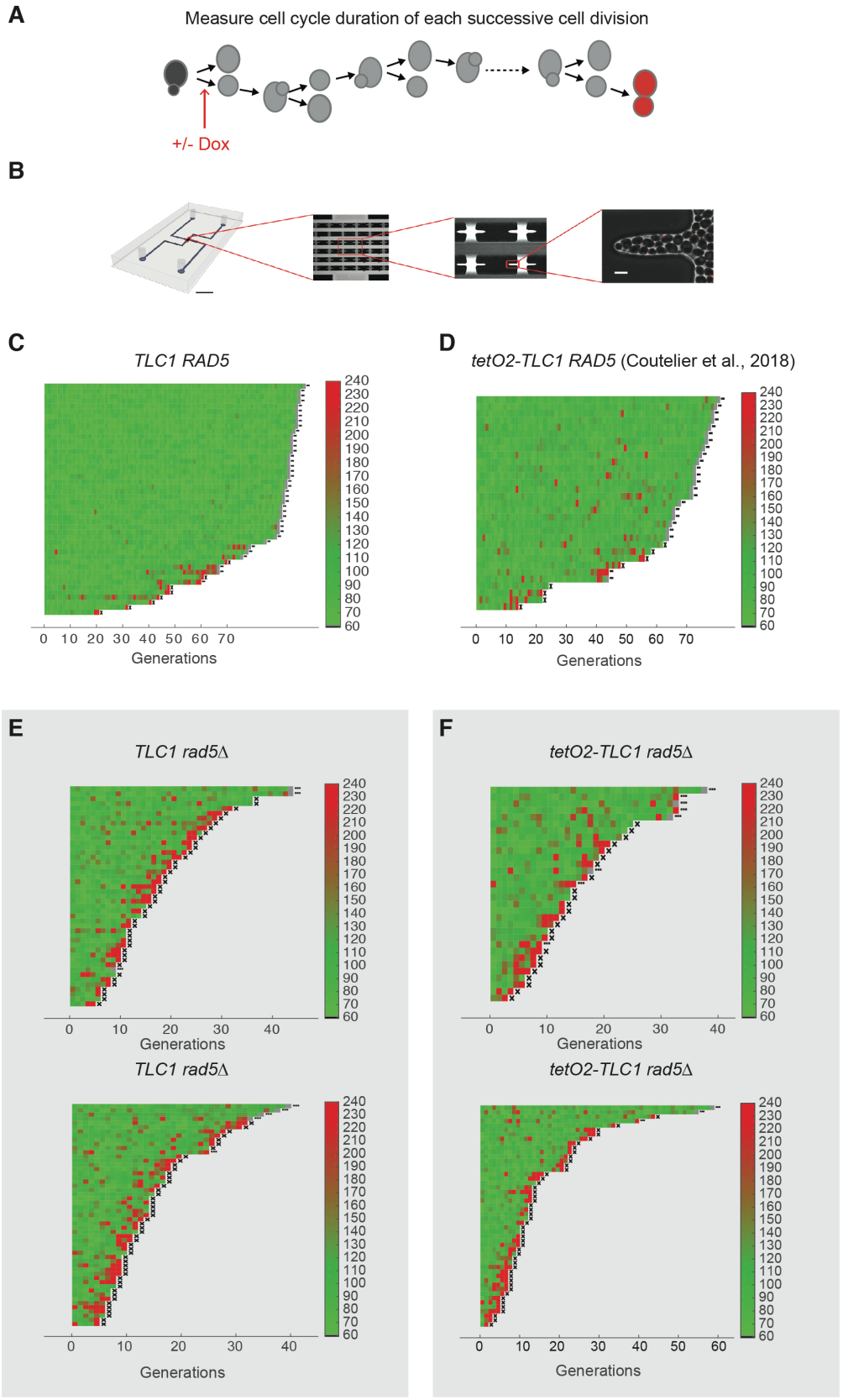

Appendix Figure

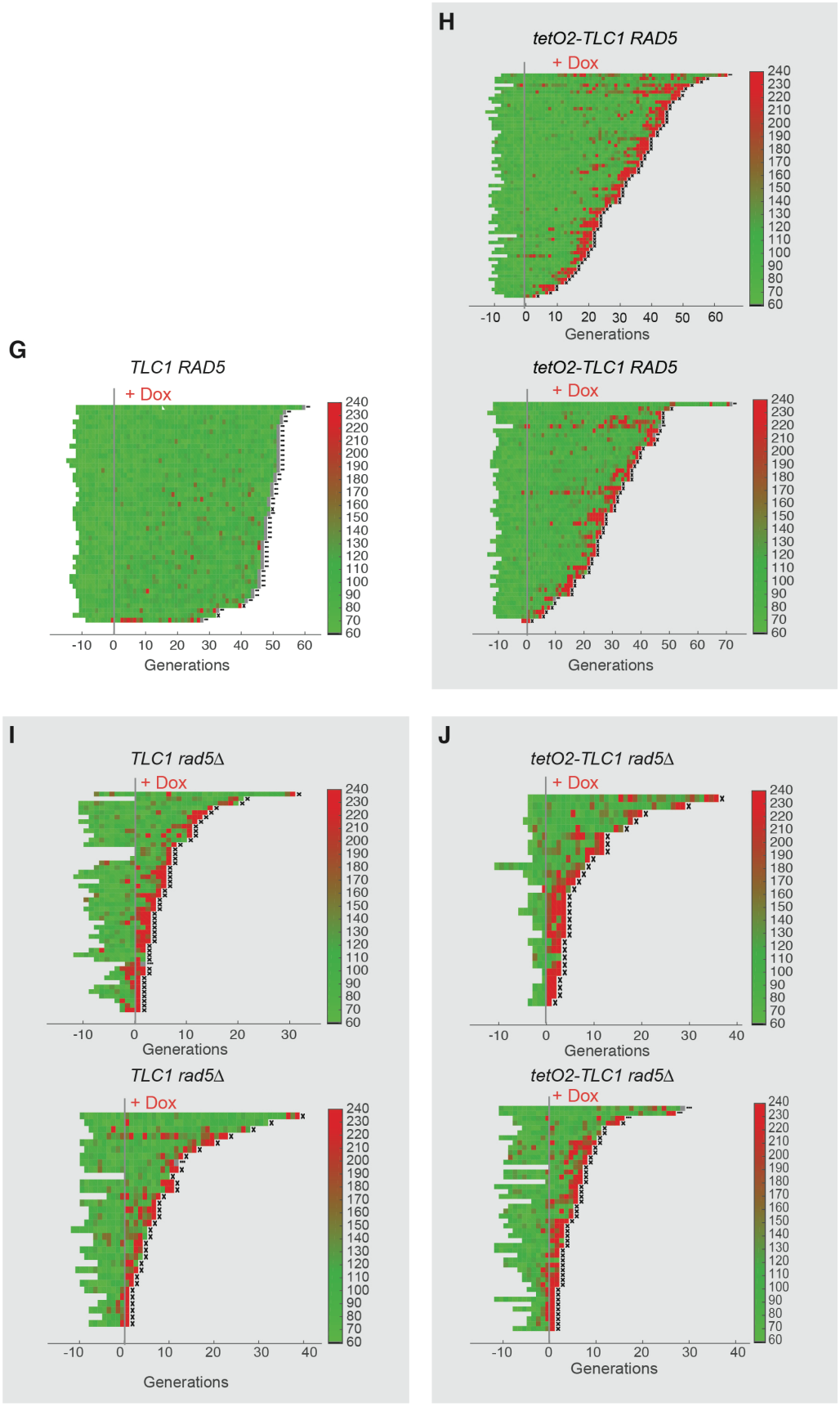

Appendix Figure (continued)

K

strain/treatment	average cell cycle length (min)	mortality rate	
TLC1 RAD5	76.91 (+/- 0.48)	<0.0021	
TLC1 RAD5 + Dox	87.22 (+/- 0.49)	<0.0021	
TLC1 rad5Δ	105.44 (+/- 1.47)	0.0594	(0.0489-0.0719)
TLC1 rad5Δ + Dox	116.43 (+/- 1.85)	0.0675	(0.0571 - 0.0797)
tetO2-TLC1 RAD5	90.70 (+/- 0.87)	<0.0041	
tetO2-TLC1 RAD5+ Dox	101.93 (+/- 0.88)	0.0342	(0.0295 - 0.0396)
tetO2-TLC1 rad5Δ	105.31 (+/- 1.96)	0.0623	(0.0504 - 0.0767)
tetO2-TLC1 rad5Δ + Dox	118.47 (+/- 2.65)	0.1186	(0.0831 - 0.1668)

Appendix Figure (continued)

Appendix Figure: *rad5Δ* cells have a high mortality rate

(A) To evaluate growth capacity of cells in presence or absence of telomerase and in different genetic backgrounds, we measure the exact duration of each consecutive cell cycle in individual lineages. (B) For this, we use a microfluidics device in which budding yeast cells grow for up to one hundred generations, allowing for the precise tracking of pedigrees. Here we show an image of the microfluidics chip, the design of the chambers and microcavities. Scale bars: 5 mm (black) and 5 µm (white) (adapted from (Xu *et al.*, 2015)). (C-J) Display of consecutive cell cycle durations of individual lineages with indicated genotypes grown in the microfluidic device obtained in one or two independent experiments using two independent transformants of *RAD5* deletion (when applicable). In (C), data is taken from (Coutelier *et al*, 2018; Xu *et al.*, 2015). Cells were monitored overnight before (-dox) and then for successive generations after (+dox) addition of doxycycline (30 µg/mL) to inactivate telomerase (designated generation 0). In experiments in which doxycycline is not added, 0 corresponds to the beginning of the movie after injection of cells and invasion of microcavities. Each horizontal line is an individual cell lineage and each segment is a cell cycle. Cell cycle duration (min) is indicated by the color bar on the side. X at the end of the lineage indicates cell death, whereas an ellipsis (…) indicates that the cell was alive at the end of the experiment. (K) Average duration of cell cycles and mortality rates per cell division calculated for indicated experimental conditions. The mortality rate is calculated as

the fraction of cell deaths over total number of cell divisions among lineages, and the 95% confidence interval of a proportion was determined using the Wald method.

We observe in this figure that switching the promoter of *TLC1* for *TetO2* has minimal consequences on cell viability in presence or absence of *RAD5* in conditions where doxycycline is not added (and expression of *TLC1* not repressed) (panels C-F), although displaying shorter telomeres (260 bp in average, instead of 300-400 bp in wt strains (Xu *et al.*, 2015)). Addition of doxycycline in cells harbouring a native promoter for *TLC1* has no effects in viability either (panel G). In contrast, deletion of *RAD5* raises the mortality rate from ~0.2% and ~0,4% in *TLC1* and P_{TetO2}-*TLC1*, respectively, to ~6%, while the average cell cycle duration increases to about 105 min (panel K). Therefore, the increase in doubling time of *rad5Δ* strains results mainly from increased mortality. When telomerase is inactivated by addition of doxycycline in P_{tetO2}-*TLC1* cells, senescence phenotype become apparent with generations as expected (panel H). Deletion of *RAD5* in these conditions did have a strong effect, but not stronger than in *TLC1* cells, in which doxycycline has no effect on telomerase (panels I-J). We conclude that the mortality rate in *rad5Δ* cells ends cell lineages way before telomerase inactivation shows effects, precluding any definitive conclusion on the genetic interactions between *TLC1* and *RAD5* with this highly sensitive technology.

Appendix Materials and Methods for the microfluidics analyses (adapted from (Xu *et al.*, 2015))

The microfluidic mold was fabricated using standard soft lithography techniques. In brief, polydimethylsiloxane (PDMS; Sylgard 184) and curing agent were mixed in a 10:1 ratio, degassed it with a vacuum pump for 30 min, and poured it into the mold. The PDMS was cured by baking at 70°C for 5 h and then removed from the mold. A biopsy puncher (1.5 mm, Harris Unicore) was used to create holes for medium flow. The surfaces of PDMS and a glass coverslip (24 × 50 mm) were surface activated using a plasma cleaner (Diener Electronic, Germany) to covalently bond the two elements. For injection of cells into the device, synthetic complete medium containing 2% glucose (SD) was filtered using a 0.22-µm polyethersulfone filter (Corning) and loaded into the device using a peristaltic pump (IPCN, Ismatec). Cells from a log-phase culture (0.5 OD_{600}) were injected into the device using a 1 ml syringe. A constant medium flow (28 µl/min) was maintained throughout the experiment.

For experiments with strains expressing the TetO2-*TLC1* construct, cells were allowed to divide and invade the cavities for 12–24 h before the medium was switched to SD containing 30 µg/ml doxycycline. Cells in the microfluidic device were imaged using a fully motorised Axio Observer Z1 inverted microscope (Zeiss), with constant focus maintained with focus stabilisation hardware (Definite focus, Zeiss). LED light sources for phase contrast were used with the following parameters: 4.0 V – 70 ms. The temperature was maintained at 30°C with a controlled heating unit and an incubation chamber that held the entire microscope base, including the stage and the objectives. Images were acquired every 10 min using 4Zen (Zeiss). A custom software written in Matlab, named SingleCellTracer, was developed in this work to allow a semi-automated analysis of cell division dynamics of individual lineages. In brief, an input microscopy movie can be directly analyzed through the user interface allowing manual detection of cell budding, divisions, as well as correction of mistakes and simultaneous monitoring of several features over time. Time-lapse images were exported as avi files and analysed directly with the graphical user interface of SingleCellTracer. To efficiently track lineages, in which we frequently switched focus from a given cell to its daughter cell, the time-lapse images were retrospectively analysed starting from the last image. This avoided tracking of lineages in which the cells were ejected from the microcavity. All computational and statistical analyses were performed in Matlab. SingleCellTracer and the functions developed in this study are available on request.

Appendix Table 1: Strains used in this study

Strain	Figure	Genotype
G49 (W303)#		*Mat a ura3-1 trp1-1 leu2-3,112 his3-11,15 can 1-100 RAD5*
yT649*	EV2, 3, EV3	G49 *rad5::HIS3MX6*
yT650*	2, EV2	G49 *mms2::HIS3MX6*
yT651	EV2	G49 *ubc4::HIS3MX6*
yT652*	2, EV2	G49 *ubc13::HIS3MX6*
yT656*		G49 *RAD5-3'-UTR::HIS3MX6*
yT695*	2, EV2	G49 *rad5-GAA-3'-UTR::HIS5*
yT696*	2, EV2	G49 *rad5-I916A-3'-UTR::HIS5*
yT717*	EV2	G49 *POL30-3'-UTR::kLEU2*
yT745*	2, EV2	G49 *rad5-AA-3'-UTR::HIS5*
yT747*	3, EV3	G49 *pol30-K164R-3'-UTR::kLEU2*
yT749*	EV2	G49 *pol30-K107R-3'-UTR::kLEU2*
yT755*	EV2	G49 *rad30::HIS3MX6*
yT756*	2, EV2	G49 *rev1::HIS3MX6*
yT757*	EV2	G49 *rev3::HIS3MX6*
yT758*	3	G49 *rad5::HIS3 pol30-K164R-3'-UTR::kLEU2*

yT769		*Mat α ura3-1 trp1-1 leu2-3,112 his3-11,15 can 1-100 RAD5 tlc1::PralphaNat pCEN-ARS-TRP1-TLC1 (pSD107)*
yT800	3, EV3	G49 *srs2::kLEU2*
yT801*	3, EV3	G49 *srs2::kLEU2 rad5::HIS3MX6*
yT811	EV3	G49 *rad5::RAD5-13xMYC-TRP*
yT752	1	G49 *bar1::kLEU2 tlc1::KANMX6-P$_{TetO2}$-TLC1 rad5::His3*
yT1185	1, EV1, 5, 5EV5	G49 *bar1::kLEU2 tlc1::KANMX6-P$_{TetO2}$-TLC1 rad5::RAD5-13xMYC-TRP1*
yT1190	5, EV5	G49 *bar1::NATMX6 tlc1::KANMX6-P$_{TetO2}$-TLC1 rad5::HIS3 srs2::kLEU2*
yT868	3, EV3	G49 *rad51::kLEU2 rad5::HIS3*
yT898	3, EV3	G49 *rad51::kLEU2*
yT1026	3, 4C	*Mata/alpha ura3-1/ura3-1 trp1-1/trp1-1 leu2-3,112/leu2-3,112 his3-11,15/his3-11,15 can1-100/can1-100 TLC1/tlc1::PralphaNat RAD5/rad5::HIS3 SRS2/srs2::TRP1 RAD51/rad51::kLEU2*
yT860	EV3	G49 *SRS2-3'-UTR-kLEU2*
yT867	EV3	G49 *SRS2-3'-UTR-kLEU2*
yT1164	4B, EV4A	G49 *leu2::P$_{GAL}$-HO mat1::loxP ade2::loxP lys2::loxP mnt2::LYS2 tlc1::HIS3MX6-P$_{TetO2}$-TLC1 mnt2::TG80-HO-CA80 ADE2*
yT1386	4B, EV4A	G49 *leu2::P$_{GAL}$-HO mat1::loxP ade2::loxP lys2::loxP mnt2::LYS2 tlc1::HIS3MX6-P$_{TetO2}$-TLC1 mnt2::TG80-HO-CA80 ADE2 rad5::TRP1*
yT1374	4B, EV4A	G49 *leu2::P$_{GAL}$-HO mat1::loxP ade2::loxP lys2::loxP mnt2::LYS2 tlc1::HIS3MX6-P$_{TetO2}$-TLC1 mnt2::TG80-HO-CA80 ADE2 rad5::TRP1 srs2::HPH*
yT1384	4B, S4A	G49 *leu2::P$_{GAL}$-HO mat1::loxP ade2::loxP lys2::loxP mnt2::LYS2 tlc1::HIS3MX6-P$_{TetO2}$-TLC1 mnt2::TG80-HO-CA80 ADE2 rad5::TRP1 srs2::HPH rad5::TRP1*
yT1175	Fig 4B, S4A	G49 *leu2::P$_{GAL}$-HO mat1::loxP ade2::loxP lys2::loxP mnt2::LYS2 tlc1::HIS3MX6-P$_{TetO2}$-TLC1 mnt2::TG250-HO-CA250 ADE2*
yT1387	Fig 4B, S4A	G49 *leu2::P$_{GAL}$-HO mat1::loxP ade2::loxP lys2::loxP mnt2::LYS2 tlc1::HIS3MX6-P$_{TetO2}$-TLC1 mnt2::TG250-HO-CA250 ADE2 rad5::TRP1*
yT1375	Fig 4B, S4A	G49 *leu2::P$_{GAL}$-HO mat1::loxP ade2::loxP lys2::loxP mnt2::LYS2 tlc1::HIS3MX6-P$_{TetO2}$-TLC1 mnt2::TG250-HO-CA250 ADE2 srs2::HPH*
yT1385	Fig 4B, S4A	G49 *leu2::P$_{GAL}$-HO mat1::loxP ade2::loxP lys2::loxP mnt2::LYS2 tlc1::HIS3MX6-P$_{TetO2}$-TLC1 mnt2::TG250-HO-CA250 ADE2 srs2::HPH rad5::TRP1*
yT1420	Fig 4C, S4B	G49 *leu2::P$_{GAL}$-HO mat1::loxP ade2::loxP lys2::loxP mnt2::LYS2 tlc1::HIS3MX6-P$_{TetO2}$-TLC1 mnt2::TG80-HO-CA80 ADE2 RAD5-Myc-TRP1*
yT1421	Fig 4C, S4B	G49 *leu2::P$_{GAL}$-HO mat1::loxP ade2::loxP lys2::loxP mnt2::LYS2 tlc1::HIS3MX6-P$_{TetO2}$-TLC1 mnt2::TG250-HO-CA250 ADE2 RAD5-Myc-TRP1*
yT1422	Fig 4D, S4C	G49 *leu2::P$_{GAL}$-HO mat1::loxP ade2::loxP lys2::loxP mnt2::LYS2 tlc1::HIS3MX6-P$_{TetO2}$-TLC1 mnt2::TG80-HO-CA80 ADE2 SRS2-Myc-TRP1*
yT1423	Fig 4D, S4C	G49 *leu2::P$_{GAL}$-HO mat1::loxP ade2::loxP lys2::loxP mnt2::LYS2 tlc1::HIS3MX6-P$_{TetO2}$-TLC1 mnt2::TG250-HO-CA250 ADE2 SRS2-Myc-TRP1*

#: Obtained from M. Lisby

*: These strains were crossed with yT769 to generate diploids for senescence spot assays.

Appendix Table 2: Primers used in this study

Name	Sequence
oT230 deletion of *RAD5* (yT649, yT752, yT867 yT1190)	5'-TAC AAA GTT ACA TTA TCA AAA GGC CTT AGA AAC ACA CCT AAA GTC TTA CAG TAT CAC AAT CGG ATC CCC GGG TTA ATT AA-3'
oT231 deletion of *RAD5* (yT649, yT752, yT1190)	5'-AGT TCT TTC GGG TTG AAA ATA ATA ATA AAT AAA GTC TTT ATA TAT GAG TAT GTG GTA TGA GAA TTC GAG CTC GTT TAA AC-3'
oT234 deletion of *MMS2* (yT650)	5'-GTC GTG GTG AAA TTC TTA TTC TGT ATA TGC AAC GTA GAA GAA AGC AGC GTT TAC ACA AAA CGG ATC CCC GGG TTA ATT AA-3'

oT235 deletion of *MMS2* (yT650)	5′-TTG CTT GTA TAT ATG AGT GGC TTG GAA TGC TGC AAA TAC TGT TTA GGA AAA AGT AGA TAA GAA TTC GAG CTC GTT TAA AC-3′
oT612 deletion of *UBC4* (yT651)	5′-TAA ATT TCA CTG ACT ATA GAG TAC ATA CAT AAA CAA GCA TCC AAA AAA ACC GGA TCC CCG GGT TAA TTA A-3′
oT613 deletion of *UBC4* (yT651)	5′-AAT CCC ATA TAA ATC TTG CTT CTC TTT TTC AGC TGA GTA AGG ACT TCT GTG AAT TCG AGC TCG TTT AAA C-3′
oT608 deletion of *UBC13* (yT652)	5′-TTT TTC CAA TAT TAG CAA ATA AGG TCA GGT TCA TTG TAA CAT AGT TAG AAC GGA TCC CCG GGT TAA TTA A-3′
oT609 deletion of *UBC13* (yT652)	5′-GTA ATG ATA TAT ATT TAT ATA TTC AGT TGA GAA AAC TTA TAC AGA AAT GAG AAT TCG AGC TCG TTT AAA C-3′
oT637 marker HIS3MX6 at 3′ UTR of *RAD5* (yT656)	5′-TAT TTA TTA TTA TTT TCA ACC CGA AAG AAC TAA TTA TTC TTC AGC TAC TCG GAT CCC CGG GTT AAT TAA-3′
oT638 marker HIS3MX6 at 3′ UTR of *RAD5* (yT656)	5′-CAA CTT AAA AAT ACG GGT AAC GGA AAA GGA AGA TAA TAG AAG TTG CAT GAG AAT TCG AGC TCG TTT AAA C-3′
oT639 *rad5-GAA* point mutation (yT695)	5′-AGG GTG GCA TAT TAT CAG ATG AAA TGG GGT TGG GTG CAG CAG TGG CAG CGT ATT CTT TAG TTT TAT CTT G-3′
oT640 *rad5-I916A* point mutation (yT696)	5′-TCC AGA CAA TAA ATC GTT TCA GTC CTT AGA GTG CTC CGC CTG CAC AAC GGA ACC TAT GGA TTT GGA CAA G-3′
oT673 kLEU2 marker at 3′ UTR of *POL30* (yT717)	5′-AAT AAT AAA CAA AAA AAA AAC AGT AAA GTT TGT TTT AAA TGA AAA TAA ATC GGA TCC CCG GGT TAA TTA A-3′
oT674 kLEU2 marker at 3′ UTR of *POL30* (yT717)	5′-TCA CAC AAA AAG CTG ATA TTT AAC GCA TCT TAG TCT TTA TTT TCT TTG TTG AAT TCG AGC TCG TTT AAA C-3′
oT681 *rad5-AA* point mutation (yT745)	5′-TTC AGG CTT ATT TTC TGT CAA TTT TTA TCG CAT AAT AAT CGC CGC CGG TCA TAA CAT TAG AAA CAG AAC GAC AGT TAC AT-3′
oT 675 *pol30-K164R* point mutation (yT747)	5′-GTC CCA ATT GAG TGA TTC TAT TAA TAT CAT GAT CAC CCG Aga aac aat aaa gtt tgt agc tga cgg tga t-3′
oT679 *pol30-K107R* point mutation (yT749)	5′-ACA CAC CGG ATT CCA TCA TCT TAT TAT TTG AGG ATA CCA GGA AAG ACC GTA TAG CCG AAT ACT CTC TGA AAT TGA TGG AT-3′
oT770 *RAD30* deletion (yT755)	5′-TAG CGC AGG CCT GCT CAT TTT TGA ACG GCT TTG ATA AAA CAA GAC AAA GCC GGA TCC CCG GGT TAA TTA A-3′
oT771 *RAD30* deletion (yT755)	5′-ATC AGG ACG TTT TAG TTG CTG AAG CCA TAT AAT TGT CTA TTT GGA ATA GGG AAT TCG AGC TCG TTT AAA C-3′
oT774 *REV1* deletion (yT756)	5′-ACA GAT TTT CTC AAA ATA AAT CGA TAC TGC ATT TCT AGG CAT ATC CAG CGC GGA TCC CCG GGT TAA TTA A-3′
oT775 *REV1* deletion (yT756)	5′-TTC GCA AAC TGC GTG TTT ACT GTA TGC TGA AAT GTT TTT TTT TTT TTA ATG AAT TCG AGC TCG TTT AAA C-3′
oT778 *REV3* deletion (yT757)	5′-ATT TGA GTC AAT ACA AAA CTA CAA GTT GT GGC GAA ATA AAA TGT TTG GAA CGG ATC CCC GGG TTA ATT AA-3′
oT779 *REV3* deletion (yT757)	5′-ATA GAA ACA AAT AAC TAC TCA TCA TTT TGC GAG ACA TAT CTG TGT CTA GAG AAT TCG AGC TCG TTT AAA C-3′
oT436 *SRS2* deletion (yT800, yT810, yT1190)	5′-ATA ATT GTA CTC TGC ACT TTG AGT ATC ATT CCA ATT TGA TCT TTC TTC TAC CGG TAC TTA GGG ATA GCA ACG GAT CCC CGG GTT AA TTA A-3′
oT437 *SRS2* deletion (yT800, yT810, yT1190)	5′-CTC CTA TGT GCT TTA AAT AAA AAT TAT AAA CCG CCT CCA ATA GTT GAC GTA GTC AGG CAT GAA AGT GCT AGA ATT CGA GCT CGT TTA AAC-3′
oT352 Tagging Rad5-MYC or GFP (yT811, yT812, yT813, yT1185, yT1362)	5′-AGT TCT TTC GGG TTG AAA ATA ATA ATA AAT AAA GTC TTT ATA TAT GAG TAT GTG GTA TGA GAA TTC GAG CTC GTT TAA AC-3′
oT354 Tagging Rad5-MYC or GFP (yT811, yT812, yT813, yT1185, yT1362)	5′-GAC ACA GAC GAA GAC GAG AGA AGA AAA AGG AGA ATT GAA GAA ATC CAG ATG CTG TTT GAA CGG ATC CCC GGG TTA ATT AA-3′
oT965 kLEU2 marker at 3′ UTR of *SRS2* (yT860)	5′-GCC TGA CTA CGT CAA CTA TTG GAG GCG GTT TAT AAT TTT TAT TTA AAG CAC GGA TCC CCG GGT TAA TTA A-3′
oT966 kLEU2 marker at 3′ UTR of *SRS2* (yT860)	5′-CCA CAT TTC CAT GTA GTT CGT ATA CAA ACC CTA CCA GTA AAA TAA AAT TAG AAT TCG AGC TCG TTT AAA C-3′

oT964 *SRS2*-deltaSIM (yT866)	5′-TTT GGC TGA CGC AGC AAT GAA AAA GAC ACA GAA ATT TTC CAA AAA GGT GAA GAA TGA ACC TGC ATC AAG TTA GTA GCA CTT TCA TGC CTG ACT ACG TCA A-3′
oT323 Deletion of *RAD51* (yT868, yT898)	5′-TTC TTC TAT CTT CCG TAG TTT CCA TAT ACT AGT AGT TGA GTG TAG CGA CAC GGA TCC CCG GGT TAA TTA A-3′
oT324 Deletion of *RAD51* (yT868, yT898)	5′-GGA TGG AAA TGA AGA TAA AAA TGT ACG GAA CGC AAC CTA AGA AAA AGA GGG AAT TCG AGC TCG TTT AAA C-3′
oT1265 Telo15L Fwd	5′-ATC GTG GTT CGC TGT GGT AT-3′
oT1266 Telo15L Rev	5′-AAC CCT GTC CAA CCT GTC TCC-3′
oT1267 Telo6R Fwd	5′-TCC GAA CTC AGT TAC TAT TGA TGG AA-3′
oT1268 Telo6R Rev	5′-CGT ATG CTA AAG TAT ATA TTA CTT CAC TCC ATT-3′
oT1269 *ACT1* Fwd	5′-AAG CCG GTT TTG CCG G – 3′
oT1270 *ACT1* Rev	5′-TTG TGT CTT GGT CTA CCG ACG- 3′
oT1392 ARS607 Fwd	5′-TCT GAA CTG CAA ATT TTT GTC ATA-3′
oT1393 ARS607 Rev	5′-AGC CTT GTG CAG AAA GCA AA-3′
oT1394 ARS522 Fwd	5′-CGT TCG AAA ACC GGA TAT GT-3′
oT1395 ARS522 Rev	5′- CCC GAT GAC TAC GAG GCT AT-3′